A Microscopic Model for the Reinforcement and the Nonlinear Behavior of Filled Elastomers and Thermoplastic Elastomers (Payne and Mullins Effects)

Samy Merabia,[†,§] Paul Sotta,[†,‡,⊥] and Didier R. Long*[,†,‡,⊥]

Laboratoire de Physique des Solides, CNRS and Université de Paris XI, Bat. 510, 91405 Orsay Cédex, France, and Laboratoire Polymeres et Matériaux Avancés, CNRS/Rhodia, 85 avenue des Freres Perret, F-69192 Saint-Fons, France

Received July 1, 2008; Revised Manuscript Received September 2, 2008

ABSTRACT: We extend a model regarding the reinforcement of nanofilled elastomers and thermoplastic elastomers. The model is then solved by numerical simulations on mesoscale. This model is based on the presence of glassy layers around the fillers. Strong reinforcement is obtained when glassy layers between fillers overlap. It is particularly strong when the corresponding clusters—fillers + glassy layers—percolate, but it can also be significant even when these clusters do not percolate but are sufficiently large. Under applied strain, the high values of local stress in the glassy bridges reduce their lifetimes. The latter depend on the history, on the temperature, on the distance between fillers, and on the local stress in the material. We show how the dynamics of yield and rebirth of glassy bridges account for the nonlinear Payne and Mullins effects, which are a large drop of the elastic modulus at intermediate deformations and a progressive recovery of the initial modulus when the samples are subsequently put at rest, respectively. These mechanisms account also for dissipative properties of filled elastomers. In particular, our results allowed also for explaining semiquantitatively the results obtained by Payne in his 1963 study. Our model opens the way for predicting mechanical behavior of nanofilled elastomers according to the filler structures and dispersion, polymer−filler interactions, and temperature, in order to prepare systems with tailored properties.

I. Introduction

Filled elastomers are systems of very great practical importance due to their unique properties. Nonreinforced polymer matrices generally do not exhibit mechanical properties suitable for practical purposes, being too soft and fragile.[1] On the contrary, elastomers filled with carbon black or silica particles have a shear modulus much (up to a few 100 times) higher than that of the pure elastomer, exhibit a high dissipative efficiency, and are extremely resistant to both fracture and abrasion, which makes them essential for damping materials, shock absorbers, or tires.[1−10] According to their potential use, their properties can be optimized in order to meet various criteria. For some purposes, such as biomedical or mechanical applications, they must have a high resistance to fatigue and, for instance, retain their initial shape even after a great number of deformation cycles.[11,12] For some other applications, they must have a very high resistance to tear and wear.[2,10] Reinforcement data published by Payne,[8] which were obtained in carbon black reinforced elastomers, are plotted in Figure 1. The modulus increases by a factor larger than 200 as the filler volume fraction increases from 0 (pure rubber) up to 38%. As will be discussed later, this phenomenon cannot be explained by purely geometrical arguments. Another important feature of filled elastomers is their nonlinear behavior in the nondestructive regime. When submitted to deformations of the order of a few percent or more, the elastic modulus decreases down to values much smaller than the initial one: this is the so-called Payne effect. For instance, in the systems studied by Payne at 38% filler volume fraction,[2,5,8] the elastic modulus drops from 5.0×10^7 Pa down to about 3.0×10^6 Pa at 30% deformation amplitude. Note that the modulus of the pure rubber matrix is 2.0×10^5 Pa in those systems. At 23% filler volume fraction, the modulus drops from 10^7 Pa down to 10^6 Pa; that is, at medium and large amplitudes, it drops into a range of values that can be accounted for by the steric effect of the fillers. In his 1963 paper, Payne showed that for the systems considered the loss modulus exhibits a peak up to 7×10^6 Pa at deformations of typical amplitude 1%, which is a key feature of strongly reinforced systems. In less reinforced systems, i.e., for smaller filler volume fraction, the peak is less pronounced. The corresponding data are plotted in Figure 2. This peak is associated with a large value of the loss tangent tan δ, at somewhat larger deformation amplitudes.

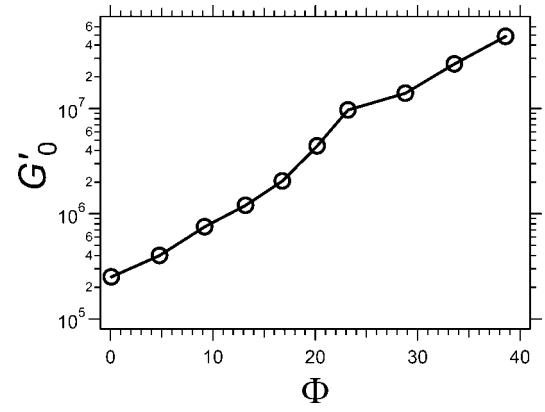

Figure 1. Elastic modulus G'_0 in the linear regime (in Pa) measured in carbon black filled butyl rubbers (polyisobutylene) as a function of the filler volume fraction Φ. After ref 8. The modulus increases continuously as Φ increases. A reinforcement $R = G'_0/G'_{\text{rubber}}$ (where G'_{rubber} is the modulus of the pure rubber, measured at $\Phi = 0$) of more than 200 is obtained at $\Phi = 38\%$.

Another important feature is that the modulus stays at lower values during subsequent deformations and that this drop of modulus can be—at least partially—recovered over time: this last feature is the so-called Mullins effect.[5,13] These features

* Corresponding author. E-mail: didier.long-exterieur@eu.rhodia.com.
† CNRS and Université de Paris XI.
‡ CNRS/Rhodia.
§ Present address: LPMCN, Université Lyon I.
⊥ Present address: CNRS/Rhodia, Saint-Fons.

10.1021/ma8014728 CCC: $40.75
Published on Web 10/14/2008

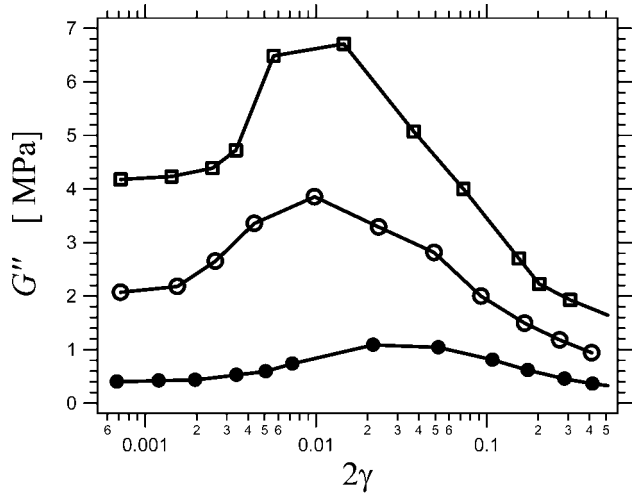

Figure 2. Loss modulus G'' (in MPa) measured in carbon black filled butyl rubbers as a function of the deformation amplitude and three different filler volume fraction: □, $\Phi = 38.6\%$; ○, $\Phi = 33.6\%$; ●, $\Phi = 23.2\%$. After ref 8.

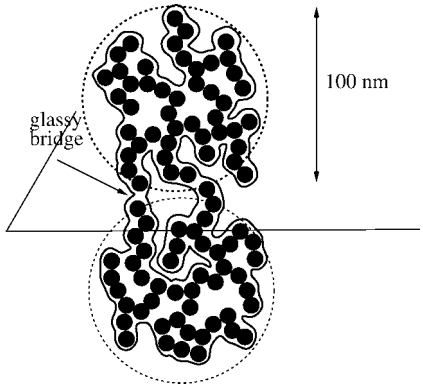

Figure 3. Macroscopic stress is supported by the glassy polymer fraction which bridges two neighboring filler aggregates. Aggregates of about 100 nm made of primary particles of 10 nm are schematically represented here. Aggregates are surrounded by a glassy layer which is roughly represented. The fraction of glassy polymer in a section normal to the applied stress is $\Sigma \sim 1\%$. The macroscopic deformation is amplified in between fillers by a factor typically $\lambda \sim 10$, which results in a macroscopic modulus G' of order to 10^7-10^8 Pa.

are of primary importance in e.g. tires applications, as regards rolling resistance, grip, and durability.[10] It is thus an issue of major importance to understand this unique behavior in order to be able to control and tune the properties of these systems.

Carbon black filled elastomers have long been used and studied. Their properties remain the subject of fundamental studies, however. Silica filled elastomers have appeared more recently. Both systems are used in tire applications.[1−3,10] In many applications, the fillers are obtained by assembling more or less spherical nanoparticles of typical diameter 10 nm (so-called primary particles) into fractal aggregates of typical diameter 100 nm (see Figure 3). A wide range of grades with various primary particle diameters and aggregate sizes and structures are available, for both carbon black and silica fillers. On the other hand, the progress of chemical synthesis and chemical engineering has allowed for the designing of very diverse nanostructured polymer materials, such as those based of block copolymers,[14,15] which exhibit a great diversity of microphase strcutures. Thermoplastics elastomers, which are of concern here, are made of e.g. ABA triblock copolymers corresponding to the so-called spherical morphologies, with nodules of A polymer embedded in a continuous matrix of B polymers. These systems behave as reinforced rubbers when the A polymer is glassy at room temperature whereas the B polymer has a low glass transition temperature T_g and is in the rubbery state at room temperature. In practice, these systems cover a wide range of elastic properties, with e.g. a shear modulus which cover the range of 10^4 Pa to 10^7 or 10^8 Pa.[15]

Predicting the mechanical properties of filled elastomers or of soft thermoplastic elastomers based on their nanostructure is a challenge of both fundamental and applied importance. When dealing with the elastic properties of these systems, theoretical models are faced to a number of difficulties, of various origins. First, microscopic reorganizations in strained rubbers are very complex,[16,17] involving excluded volume interactions, nonaffine displacements of the cross-links and trapped entanglements, and dangling ends. In filled elastomers, the presence of filler particles introduces additional issues. An important feature is the shift of the glass transition temperature induced by the presence of the fillers. Indeed, it has long been proposed that the polymer matrix in the vicinity of the filler is glassy.[18−24] This picture is consistent with experimental studies which demonstrated that the glass transition temperature T_g in polymer thin films in contact with a solid substrate differs from that in the bulk, with a sign of the effect depending on the polymer−substrate interaction.[25−34] For strong polymer/substrate interactions, an increase of T_g is reported, which implies that a polymer in the vicinity of the substrate is glassy, while far from the interface the polymer is in the molten state.

Given the sensivity of the viscosity on the temperature close to T_g, these effects have a strong influence on the local rheological properties of a polymer close to an interface and thus should account for the spectacular reinforcement effects described before, as we will see later on. Indeed, Berriot et al. have shown that this glassy layer plays an essential role in the reinforcement mechanism.[35−38] As discussed later, maximum reinforcement occurs in a regime where the elastomer matrix is effectively glassy in the vicinity of the fillers. The link between glass transition in thin films and physical properties of nanocomposites has also been emphasized by many other authors.[39−50] The aim of the present article is to show how T_g shifts observed in thin films explain semiquantitatively the elastic properties of reinforced elastomers, in particular as a function of the polymer/filler interaction, the filler volume fraction, and temperature.

Given the spatial and temporal relevant scales of the problem, molecular simulations are inappropriate,[51] and a coarse-grained approach at the scale of the fillers is unavoidable. Among recent related works, let us mention the finite element mapping with spring network representations by Gusev[52] and the multiscale model of Bauerle et al.[53,54] Another mesoscale model has been introduced recently in order to deal with large scale elastic and plastic properties of filled elastomers.[55−57] The elementary length scale of the model is typically of the order 10−100 nm, depending on the filler diameter and/or on the typical distance between fillers. However, these works have been restricted to the high temperature regime, in which the glass transition shift induced by the fillers can be ignored. The purpose of this paper is to describe the mesoscale behavior of filled elastomers in the strongly reinforced regime by taking the presence of glassy layers around the fillers into acccount. Mechanical properties of filled elastomers depend in a complex way on many parameters, such as the filler volume fraction, the temperature, the quality of filler dispersion, and the structure and size of the fillers. Also, a key feature is the nature and strength of the interaction between the fillers and the matrix. A mesoscale model is proposed, which incorporates all these features and is able to predict semiquantitatively the mechanical behavior of filled elastomers in the linear regime (reinforcement) as well as in the nonlinear—but nondestructive—regime (Payne and

Mullins effects). In this article, we will describe in detail the physical model we propose, its implementation and numerical resolution, and the way in which the physical quantities are incorporated in the parameters of the simulations. It is very important to note that all the parameters of the model are based on physical, measurable quantities. The model is aimed at being generic, regarding the physical issues mentioned above and in particular regarding the fillers structure. It should apply to carbon black or silica reinforced elastomers or to thermoplastic elastomers with the relevant nanostructure as mentioned above. However, a mapping must be made between the real physical systems and the parameters used in the simulations, which we describe in this article. In particular, for simulation purposes, the perhaps complex structure of the filler have to be simplified, and we shall consider only spherical filler particles. We will discuss in details how the results of the model may be interpreted and transposed when considering more complex fillers such as fractal aggregates.

The paper is organized as follows. In section II we describe the basic features of our model and the physical mechanisms we propose to be relevant for the reinforcement and nonlinear behavior. In section III we describe how the relevant physical quantities can be translated into the input parameters of the numerical simulations. The results are presented and discussed in section IV. More details regarding the simulation method are given in the Appendix.

II. Physical Description of the Model

A. Shift of the Glass Transition Temperature T_g in the Vicinity of the Fillers. The model is based on the presence of a glassy layer around the fillers when the interaction between the matrix and the fillers is sufficiently strong. The presence of this glassy layer has been demonstrated in refs 35−37. This glassy layer has the same physical origin as the T_g shift measured in thin polymer films.[28,29,39] It has been proposed that the T_g shift at the distance z from an interface is of the form[31,34]

$$T_g(z) \approx T_g\left(1 + \left(\frac{\beta}{z}\right)^{1/\nu}\right) \quad (1)$$

where T_g is the bulk glass transition temperature of the pure rubber. $\nu \approx 0.88$. The value of the length β depends on the matrix−filler interaction. For strong interactions, it is of the order 1 nm. It follows from eq 1 that, at temperature T, the fillers are surrounded by a glassy layer of thickness e_g:[35−37]

$$e_g(T) = \beta\left(\frac{T_g}{T - T_g}\right)^{\nu} \quad (2)$$

For the sake of simplicity, we assume from now on that the T_g shift at a distance z is given by

$$T_g(z) = T_g\left(1 + \frac{\beta}{z}\right) \quad (3)$$

and that the glassy layer thickness as a function of T can be calculated accordingly. Let us discuss typical values of the parameter β in the regime of interest. In a film with strong substrate/polymer interactions, the increase of T_g can be as large as 50 K at a distance of 10 nm.[25−27] This corresponds to a value of β of 1.5 nm. For $\beta \sim 1$ nm and $T_g \approx 200$ K, we obtain an increase of T_g of 100 K for $z = 2$ nm, which is a typical interparticle distance for strongly reinforced elastomers as we shall see later in the paper.

Then, the proposed reinforcement mechanism is the following. At high temperature and/or moderate volume fractions, the glassy layers do not overlap, and they just amount to increase the effective filler volume fraction.[36,37] At higher filler volume fractions and/or lower temperature, the glassy layers overlap. The system then enters the strongly reinforced regime (see Figure 4). In glassy layers, the local shear modulus G' of the polymer matrix varies abruptly from 10^9 Pa (glassy modulus) close to the fillers down to $G'_{rubber} \approx 10^{5-6}$ Pa (the typical modulus of the pure elastomer matrix) over a distance of a few nanometers. Let us consider experimental results obtained by Berriot et al.[36,37] regarding reinforcement of model systems. When plotting the reinforcement, defined as the ratio $R = G'/G'_{rubber}$, where G' is the shear modulus of the filled elastomers and G'_{rubber} that of the pure rubber matrix, a strong peak is observed at a temperature $T_{peak} > T_g$. T_{peak} depends on the considered systems. In the systems studied by Berriot et al.,[37] $T_{peak} \approx T_g + 7$ K. Note that in refs 36 and 37 the typical distance between fillers was 20−30 nm, which is quite large. *The very presence of this peak, whereas fillers are separated by such large distances, demonstrates that one cannot explain reinforcement by geometrical effects and that the change of dynamics induced by the presence of a solid interface is long-ranged.* As we will see below, the temperature T_{peak} shifts to higher temperatures and the reinforcement decreases more slowly with increasing temperatures, when the distance between neighboring fillers decreases.

When glassy layers overlap, the macroscopic shear modulus G' is related to the shear modulus of the glassy polymer G'_g through geometrical effects. Indeed, a macroscopic deformation ϵ is amplified locally in between the fillers by an amplification factor λ, which is the ratio between the diameter of the fillers and the distance between two neighboring fillers. This effect tends to increase the reinforcement. In a plane normal to the direction of elongation, the stress is supported by glassy bridges which represent an area fraction $\Sigma < 1$ (see Figure 3). Reducing Σ tends to reduce the reinforcement. Both parameters λ and Σ depend on the considered systems. In principle, Σ depends also

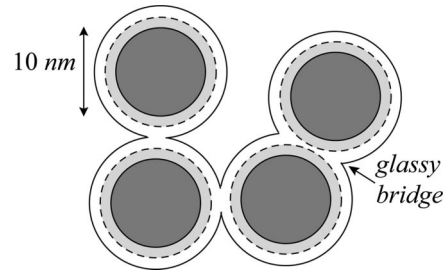

Figure 4. At low volume fractions and/or at high temperatures, the glassy layers around filler particles (light gray dashed circles) do not overlap. At lower temperature, they do overlap and build glassy bridges between fillers (plain white circles). Reinforcement then becomes much higher.

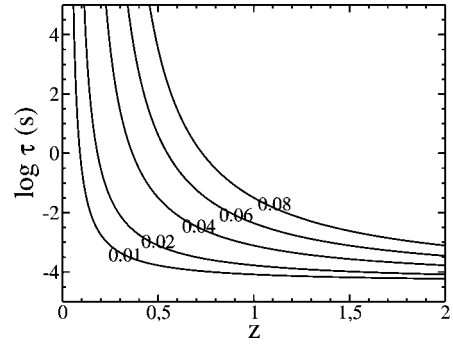

Figure 5. Breaking time (or lifetime) of glassy bridges as a function of the distance z (in units of the particle diameter) between filler particles, for a temperature $T = 243$ K, for various values of the matrix−filler interaction parameter β: $\beta = 0.01$, 0.02, 0.04, 0.06, and 0.08. The lifetime is given by eqs 6 and 1.

on temperature, but for the sake of simplicity we will consider it as a constant (for each system) in this article. The macroscopic modulus is thus given by

$$G' \approx G'_g \lambda \Sigma \tag{4}$$

Let us estimate some orders of magnitude. Assuming that the fillers are spherical particles of 10 nm diameters with typical interparticle distance of a few nanometers, we deduce that λ is of order a few units and Σ is of order a few 10^{-2}, depending on the ratio between the glassy layer thickness and the nearest-neighbor distance. Since $G'_g \sim 10^9$ Pa, we obtain a macroscopic shear modulus of about 10^8 Pa, which corresponds to very strong reinforcement. In the case of fractal, rigid aggregates of typical diameter 100 nm, made of spherical particles of 10 nm diameter, the parameter λ is of order 10, whereas Σ is smaller, e.g., $\Sigma \approx 10^{-2}$, which leads also to a modulus of order 10^8 Pa, similar to the systems considered by Payne in ref 8 (see Figure 1). Smaller values of both λ and Σ, corresponding e.g. to particles which are farther apart or have a smaller fraction of contacts to nearest neighbors (see Figure 3), lead to modulus of a few 10^6 Pa, which corresponds to a more moderate reinforcement, comparable to the systems considered in refs 58 and 59. Thus, the important point to emphasize here is that a very broad range of reinforcement values, observed in various systems, may be described by the picture proposed here.

B. Effect of an Applied Stress: Yielding of Glassy Bridges. As shown above, when a strain is applied to a strongly reinforced sample, the stress is concentrated in the glassy bridges. The *local* stress σ results in a lowering of the *local* glass transition of the polymer given by[37]

$$T_g(z,\sigma) = T_g\left(1 + \frac{\beta}{z}\right) - \frac{\sigma}{K} \tag{5}$$

The first term on the right-hand side of eq 5 represents the effect of the interaction between the fillers and the matrix as described in section IIA. The second term is the decrease of T_g due to the local stress, which is the plasticizing effect of an applied stress. K depends on the polymer. This parameter is known from macroscopic experiments. It relates the yield stress σ_y to the temperature T and the polymer glass transition temperature T_g by $\sigma_y = K(T_g - T)$. K is of the order 10^6 Pa K^{-1} typically.[60]

Let us discuss the effect of a macroscopic deformation ϵ of a few percent. The local stress σ is then of order $\sigma \sim \lambda \epsilon G'_g \sim 10^8$ Pa. With $K \sim 10^6$ Pa K^{-1},[60] a local T_g reduction of 100 K is obtained. This is comparable to the increase of T_g due to interfacial effects described in section IIA. We obtain therefore that the glassy bridges yield, which results in a lowering of the shear modulus, for macroscopic deformations of order a few percent. This is indeed comparable to the Payne effect,[8] which is a sharp decrease of the elastic modulus in this range of deformation.

C. Lifetime of Glassy Bridges: Aging. The glassy bridges are not permanent. Indeed, as we will discuss, they break under applied strain. Within a glassy bridge in between two neighboring particles, at equilibrium, we assume that the polymer has locally the dominant relaxation time τ_α given by the William−Landel−Ferry (WLF) law of the corresponding polymer,[61] modified by the T_g shift due to interfacial effects. In the reinforced elastomer at equilibrium and under no applied strain, we assume that the breaking times of glassy bridges are comparable to the local dominant relaxation times τ_α of the glassy bridges. The breaking time is thus given by

$$\log\left(\frac{\tau_{WLF}(T - T_g(z))}{\tau_g}\right) = -\frac{C_1(T - T_g(z))}{C_2 + (T - T_g(z))} \tag{6}$$

where $\tau_g = 100$ s (the relaxation time at T_g) and T is the temperature. C_1 and C_2 are the WLF parameters of the considered polymer.[61]

The breaking time of a glassy bridge between two neighboring fillers is plotted in Figure 5 as a function of the distance z between the fillers, for different values of the interaction parameter β. For $\beta \approx 0.06$, the breaking time becomes longer than experimental time scales at distances about 0.4 (in units of the filler diameter). The WLF law used here corresponds to that of polyisoprene with the parameters $T_g = 213$ K, $C_1 = 12.8$, and $C_2 = 34$ K.[62]

When a local stress σ is present, the local T_g is modified according to eq 3. Then, the breaking time is assumed to be equal to the local relaxation time $\tau_\alpha(z,\sigma)$ at equilibrium, given by

$$\log\left(\frac{\tau_\alpha(z,\sigma)}{\tau_g}\right) = \log\left(\frac{\tau_{WLF}(T - T_g(z,\sigma))}{\tau_g}\right) = -\frac{C_1(T - T_g(z,\sigma))}{C_2 + (T - T_g(z,\sigma))} \tag{7}$$

where $T_g(z,\sigma)$ is given by eq 5. Equation 7 gives the equilibrium value of the breaking time, which is obtained when the distance z, the local stress σ, and the temperature T are maintained fixed permanently. In general, the breaking time depends on the history of the glassy bridge and is denoted by $\tau_\alpha(t)$. The corresponding evolution will be discussed below. We assume that, at any time, a glassy bridge has a probability for breaking per unit time, dP/dt, given by

$$dP = \alpha \frac{dt}{\tau_\alpha(t)} \tag{8}$$

where α is a number of order 1, but smaller than 1 (see discussion below). We will assume $\alpha = 0.3-0.4$ in the following. When a glassy bridge breaks, the local stress σ is relaxed and drops to a much smaller value, which is the rubbery contribution. Immediately after breaking, we assume that τ_α relaxes to a value $\tau_{min} \sim \dot{\gamma}^{-1}$, where $\dot{\gamma}$ denotes the local deformation rate. In practice, typical deformation rates in our simulations will be of order $\dot{\gamma} = 0.1$ s^{-1}. The local breaking time $\tau_\alpha(t)$ undergoes a subsequent evolution, analogous to an aging process.[63] Thus, the evolution of the breaking time of a glassy bridge, $\tau_\alpha(t)$, is given by

$$\frac{\partial \tau_\alpha(t)}{\partial t} = 1 \tag{9}$$

if

$$\tau_\alpha(t) \le \tau_{WLF}(T - T_g(z,\sigma)) \tag{10}$$

and by definition, we set the time τ_α to be bounded by the time $\tau_{WLF}(T - T_g(z,\sigma))$ given by eq 7. Equations 8−10 describe the evolution of the local breaking time. Thus, we assume that, as the local stress increases, the breaking time drops to a smaller value and then increases progressively again when the stress decreases, up to the value set by the local glass transition temperature, which depends on the local stress and the distance between neighboring fillers. When breaking does occur, we assume that the breaking time drops to the smallest value τ_{min}, before increasing slowly again. The fact that α has to be chosen smaller than 1 is directly related to the aging dynamics (eq9). Values for α larger than or equal to 1 would not allow the system to age, which has no physical meaning. Thus, we assume that the breaking time is comparable to but larger than the α

relaxation time, which is itself comparable to the aging time (under permanent conditions).

What is important to note is that within our model there is no zero or one picture regarding the glassy bridges. Indeed, the glassy bridges are always present, though with hugely varying lifetimes and thus hugely varying effects. As we will see in section IID and in the discussion (section IV), *their effects depend indeed crucially on these lifetimes, and only on these lifetimes*. We do not consider therefore a specific time scale beyond which they might be considered as glassy and below nonglassy. However, what is important to note, as we will see in section IIC and later in the text, is that their effect is particularly important when their lifetimes reach the typical time scale of the experiment, here the period of deformation, of order 1 or 10 s. For instance, glassy bridges with much shorter time scales contribute significantly neither to the elastic modulus nor to the loss modulus. Glassy bridges with lifetimes comparable to the period contribute in a large part to the loss modulus and are responsible in particular for the peak of G''. Glassy bridges with lifetimes much larger than the period are responsible for the large value of the elastic modulus but do not contribute significantly to the loss modulus.

D. Dissipation. There are several sources of dissipation in the systems we consider. (1) The first one is the contribution of the rubbery matrix. We assume that for the systems considered in this article this contribution is not the dominant one, and we do not focus on it. This is a reasonable assumption when the matrix is well cross-linked and does not have dangling ends, for instance. (2) The second one is due to the shearing of the glassy polymer layers in between the fillers. When glassy bridges overlap and do not yield, at small deformation amplitude, the corresponding dissipation is relatively small. (3) The third source of dissipation is due to the yielding of glassy bridges: the stored elastic energy is entirely dissipated. This is a major source of dissipation in the reinforcement regimes considered in this paper. (4) The fourth one is due to the shearing of polymer layers in between the fillers, after the glassy bridges have yielded. We will see that this is also an important contribution to the total dissipation. In this regime, the local dynamical state is similar to that of a glassy polymer undergoing yielding under cold drawing. It is controlled by the local shear rate itself, and it may be assumed that the dominant relaxation time τ_α becomes comparable to the inverse of the local shear rate: $\tau_\alpha \sim \dot{\gamma}^{-1}$. This means that the local viscosity is essentially proportional to $\dot{\gamma}^{-1}$ in this regime. Indeed, rheology experiments in glassy polymers show that the stress $\eta(\dot{\gamma})\dot{\gamma}$ depends on $\dot{\gamma}$ only logarithmically and is typically of order a few 10^7 Pa.[64]

Let us discuss in more detail the respective contributions of the fourth and third dissipation mechanisms to the loss modulus G''. We consider first mechanism 4. This mechanism is present at any deformation amplitude. Indeed, glassy bridges are surrounded by polymer layers which are close to the glass transition: this is the transition zone between the deeply glassy bridges and the rubbery matrix. The fraction of material in the transition zone increases at relatively large strain amplitudes, when glassy bridges have yielded under stress. In the regime of interest, in which the macroscopic strain rate can be of order $\dot{\gamma} \approx 0.1\ s^{-1}$ and $\gamma \sim 1$, the local strain rate is amplified by the amplification factor λ (see section IIA), and the fraction of contact which dominates the friction between neighboring fillers is given by Σ. The contribution to the viscous stress is thus $\sigma_{visc} \approx \lambda\dot{\gamma}\eta(\lambda\dot{\gamma})\Sigma$, where $\eta(\lambda\dot{\gamma})$ is the strain rate dependent viscosity. Therefore, the macroscopic loss modulus $G'' = \sigma_{visc}/\gamma \sim \Sigma\eta(\lambda\dot{\gamma})\lambda\dot{\gamma}/\gamma$ in the reinforced elastomer is of order a few 10^6 Pa (for $\Sigma \sim 10^{-2}$) and $\gamma = 0.1$, which is indeed comparable to Payne's results.[8]

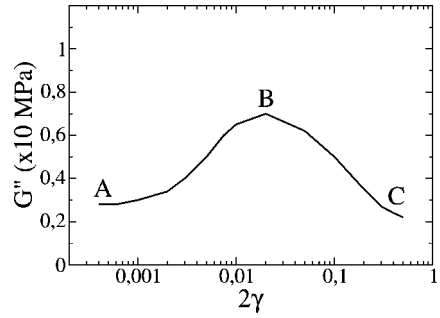

Figure 6. One may consider several regimes for the dissipation in strongly reinforced elastomers. At low deformations, the regime A is dominated by the addition of mechanism 1 (dissipation in the rubbery matrix) and mechanism 4 (dissipation in polymer close to the glass transition). Regime B is dominated by mechanism 3 (rupture and rebirth of glassy bridges). Regime C is dominated by the addition of mechanisms 1 and 4 again.

Let us consider now the contribution of glassy bridges breaking and rebirth to the dissipative power (mechanism 3). This contribution has to do with their lifetimes as well as with their capacity to build again, e.g., in an oscillatory shear experiment in permanent regime. For instance, at very large shear amplitudes, we will see that this contribution is relatively small because glassy bridges cannot build again once broken. At small deformation amplitudes, this contribution is negligible as well because no breaking takes place. On the other hand, at intermediate deformations, glassy bridges break and rebuild permanently, which leads to a large contribution to the dissipation. The dissipation (or loss modulus) will be one of the results of the simulations. Nevertheless, let us estimate orders of magnitude. Assuming that a fraction $\psi \sim 0.1$ of glassy bridges break and rebuild per period at a deformation amplitude γ_c, the resulting dissipative power is proportional to $G'(\gamma = 0)\gamma_c{}^2\psi$. We thus obtain a contribution to the loss modulus $G''(\gamma_c) = G'(\gamma = 0)\psi$ of the order a few 10^6 Pa. Given that the shear modulus has simultaneously decreased to $G'(\gamma_c) = G'(\gamma = 0)\psi$ due to the breaking of glassy bridges, the ratios of $G''(\gamma)/G'(\gamma)$ thus may be of order 1 in this regime of intermediate deformation amplitudes, as it is indeed observed experimentally.[8]

To summarize, one may consider several regimes for the dissipation in strongly reinforced elastomers exemplified in Figure 6. At low deformations, the regime A is dominated by the addition of mechanism 1 (dissipation in the rubbery matrix) and mechanism 4 (dissipation in the fraction of the polymer matrix which is close to the glass transition). At intermediate deformation amplitudes, regime B is dominated by mechanism 3: rupture and rebirth of glassy bridges. At larger deformation amplitudes, regime C is dominated by the addition of mechanisms 1 and 4 again.

III. Modelization

The model described above will be solved numerically by overdamped dissipative particle dynamics. The implementation is performed by extending a model which we proposed recently[55−57] for describing mesoscale behavior of soft thermoplastic elastomers or reinforced elastomers in the high temperature regime, when glassy layers do not overlap. The basic ingredients of the model are permanent elasticity, disorder, and excluded volume effects. The solid filler particles are represented by hard spheres randomly distributed in space.

The degrees of freedom are the centers of mass of the fillers (see Figure 4). The diameter d of the fillers sets the unit length scale. The equations of the dynamics are noninertial and include a source of dissipation in the form of a hydrodynamic friction term. The equation of motion for particle i is thus

$$\vec{F}_{\mathrm{el}}^{\,i} + \vec{F}_{\mathrm{hs}}^{\,i} + \vec{F}_{\mathrm{hydro}}^{\,i} = \vec{0} \tag{11}$$

where $\vec{F}_{\mathrm{el}}$ is the elastic force between two neighboring particles and is the sum of the contribution of the glassy bridges and of the rubbery matrix. $\vec{F}_{\mathrm{hs}}$ is the hard core repulsion, and $\vec{F}_{\mathrm{hydro}}$ is the friction force between two neighboring particles. More technical details regarding the implementation of the model into a numerical code are given in the Appendix. In this section we discuss how the physical parameters of the model can be translated into parameters for the simulations in order to solve the model numerically.

A. Elastic Forces. In addition to excluded volume interactions, two neighboring fillers interact with two distinct forces, schematized in Figure 7 and described by two types of springs: (1) permanent springs of modulus $k_\infty = 1$. In our dimensionless system, this spring constant sets the unit of modulus. For being specific we assume that it corresponds to a value of 5×10^5 Pa in the following. All the results will therefore be expressed in units of MPa. (2) Springs corresponding to glassy bridges. These springs have finite lifetimes: they break and rebuild permanently. The glassy modulus, 10^9 Pa, is typically 3 orders of magnitude or more larger than the rubbery modulus. However, because of the geometric effects mentioned in section IIA, when translated in terms of spring stiffness, this quantity has to be rescaled by the product $\lambda\Sigma$, which we choose to be 10^{-1}. The glassy spring constant is thus set to $k_0 \approx 100$. The force due to the rubbery matrix is therefore given by

$$\vec{F}(\vec{r}) = -k_\infty(\vec{r} - l_0\vec{u}) \tag{12}$$

l_0 is the equilibrium length of the springs, $\vec{r}$ is the vector joining the centers of the two particles, and $\vec{u}$ is the unit vector joining the two particles. The force due to the glassy bridges reads

$$\vec{F}_{\mathrm{g}} = -k_0(\vec{R}_{ij} - \vec{R}_{ij}^{\mathrm{ref}}) \tag{13}$$

where $\vec{R}_{ij} = \vec{R}_i - \vec{R}_j$ and $\vec{R}_i$ is the vector position of filler i. The reference state $\vec{R}_{ij}^{\mathrm{ref}}$ corresponds to the relative positions of the fillers when the last glassy bridge breaking occurred. When breaking takes place at time t (see Figure 7), the relative displacement as compared to the previous breaking, R_{ij}^{ref}, is set to the instantaneous relative position of the fillers so that $\vec{F}_g$ (eq 13) cancels at time t. Subsequent relative displacement at time $t' > t$ will be calculated according to this new reference state. The lifetimes of glassy bridges are the results of a dynamical evolution calculated according to eqs 7, 8, 9, and 10. This dynamical evolution depends on the local glass transition temperature (eq 7), which allows for calculating time scales in physical units (seconds). We thus take the local history into account in a simple way.

As discussed in the previous section, when the $T_{\mathrm{g}}(z,\sigma)$ assigned to the glassy spring remains low as e.g. during an oscillating shear experiment, the spring will break and rebirth frequently, contributing to steady state dissipation. On the other hand, if the local T_{g} keeps a high value after a breaking event, subsequent rupture will be rather unprobable; the spring lifetime increases gradually to reach values comparable to experimental time scales $\simeq$1 s, contributing to increase the overall elastic modulus.

B. Friction. In the numerical simulations, viscous dissipation is accounted for by a friction coefficient ζ^{num}, such that the viscous force between two neighboring particles i and j in our simulations is written as

$$\vec{F}_{\mathrm{hydro}} = -\zeta^{\mathrm{num}}(\vec{v}^{\,i} - \vec{v}^{\,j}) \tag{14}$$

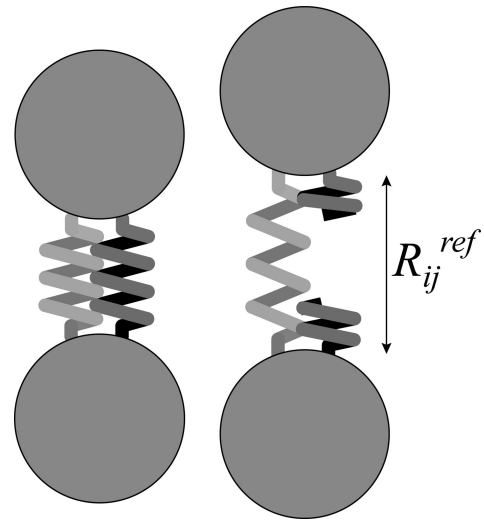

Figure 7. Modeling of a filled elastomer in the strong reinforcement regime. Two neighboring filler particles interact via two distinct forces, which correspond to (a) permanent springs of stiffness $k_\infty = 1$ representing the rubber matrix contribution and (b) nonpermanent springs due to the glassy bridges of much larger stiffness $k_0 \sim 100$, which have finite lifetimes depending on the local history, the local stress at earlier times, and the local glass transition temperature. When the local stress increases, it can lead to a breaking of a glassy bridge and the fillers take a new reference relative position R_{ij}^{ref}.

The superscript num denotes quantities used in the simulations. The relevant value of the friction coefficient ζ^{num} has to be determined according to the physics of the considered systems. For the sake of simplicity we will calibrate ζ^{num} according to the fourth dissipation mechanism discussed in section IID, corresponding to large deformation amplitudes and the frequency range studied here.

When considering real physical quantities with physical dimensions, the contribution of the dissipative force in eq 14 to the stress is $\zeta^{\mathrm{phys}}(v^i - v^j)/d^2 = \zeta^{\mathrm{phys}}\dot{\gamma}/d$, where d is the filler diameter or typical distance between fillers. The superscript phys denotes real physical quantities. This leads to $\zeta^{\mathrm{phys}}\dot{\gamma}/d = \lambda\dot{\gamma}\eta(\lambda\dot{\gamma})\Sigma$ and therefore to the relation

$$\zeta^{\mathrm{phys}} = \frac{d\lambda\dot{\gamma}\eta(\lambda\dot{\gamma})\Sigma}{\dot{\gamma}} \tag{15}$$

In the numerical simulations, the stress is measured in units of the elastic modulus G'_{rubber} of the pure rubber matrix above T_{g}. The expression for the friction coefficient ζ^{num} in the numerical simulations states that the viscous stress (expressed in units of G'_{rubber}) is the product of the friction coefficient ζ^{num} by the shear rate $\dot{\gamma}$. This relation thus reads

$$\zeta^{\mathrm{num}} = \frac{\lambda\dot{\gamma}\eta(\lambda\dot{\gamma})\Sigma}{\dot{\gamma}G'_{\mathrm{rubber}}} \tag{16}$$

where we have used here the fact that the filler diameters d sets the unit length scale. Note that the friction coefficient ζ^{num} has the dimension of a time and is expressed in seconds. The quantity $\lambda\dot{\gamma}\eta(\lambda\dot{\gamma})$ is typically of order 10^7 Pa. We assume that $\Sigma \approx 10^{-2}$, $\dot{\gamma} = 0.1\ \mathrm{s}^{-1}$, and $G'_{\mathrm{rubber}} = 5.0 \times 10^5$ Pa. It thus results that ζ^{num}, which will be denoted by ζ from now on, is of order a few seconds. Specifically, the value $\zeta = 4$ s has been chosen in the simulations.

Note that we chose here to calibrate the friction coefficient ζ in order to represent quantitatively the dissipative power in the large deformation amplitude regime. Thus, we do not aim at representing quantitatively the low strain amplitude dissipation. Extending our model for describing this regime is straighfor-

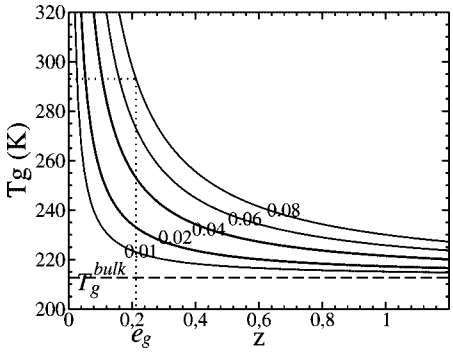

Figure 8. Local glass transition temperature $T_g(z)$ as a function of the distance z between filler particles, in units of the particle diameter, as given by eq 1, for various values of the matrix−filler interaction parameter β: $\beta = 0.01$, 0.02, 0.04, 0.06, and 0.08 (from bottom to top curve). When the temperature $T_g(z)$ is equal to the temperature T, the distance z is equal to the glassy layer thickness e_g. The dashed line is the T_g of the pure rubber. The glassy layer thickness at $T = 293$ K corresponding to $\beta = 0.08$ is indicated.

ward, however, and can be done by making the friction discussed here explicitly strain rate dependent and adding a constant friction for representing the contribution of the rubbery matrix (first contribution to the dissipative power discussed in section IID). This will be done in further extensions of this work.

C. Local T_g between Neighboring Particles. We discuss here the values to be used in the simulations for the parameters β and K as defined by eqs 3 and 5.

1. Filler−Matrix Interaction. The dimensionless value of β depends on the size of the fillers. The diameter of fillers, d, sets the unit length. If we assume a diameter of the filler of 10 nm, a value of $\beta \approx 1$ nm results in a dimensionless value of 0.1. In our simulations, this value corresponds to the case of strong interactions between the fillers and the matrix. Note that the T_g shift may be tuned to smaller values by tuning the polymer/substrate interaction.[34] In the description adopted here, varying β (in dimensionless units) amounts to varying either the filler diameter or the filler−matrix interaction. The local glass transition temperature is plotted as a function of the distance to a filler particle in Figure 8, for different values of the interaction parameter β. The thickness of the glassy layer around the fillers may thus be obtained from this plot at a given temperature and for a given interaction parameter.

2. Yield Behavior of Glassy Bridges. We consider here how to determine the constant K for describing the yield behavior of glassy bridges to be used in the simulations. We denote this constant here by K^{num}. For calculating the glassy bridges lifetime, we will work with physical time scales (in seconds) in the simulations and use the WLF law of the considered polymer. When a stress is present in a glassy bridge, the constant K^{num} must allow for calculating the corresponding T_g shift (in kelvin). Therefore, K^{num} must satisfy to the following equation:

$$\Delta T_g = -\sigma^{phys}/K^{phys} = -\sigma^{num}/K^{num} \tag{17}$$

where the subscript phys denotes real physical quantities and the subscript num denotes quantities used in the simulations. σ^{phys} is the local stress of a glassy bridge. Note that the constant K^{num} has the dimension of an inverse temperature (K^{-1}). For an applied deformation ϵ, the local numerical stress is $\sigma^{num} = k_0\epsilon$, whereas the local physical stress is given by $\sigma^{phys} = G'_g\lambda\epsilon$. Thus, we must have $K^{num} = k_0K^{phys}/G'_g\lambda$. Given that the elastic constant of the numerical simulation is $k_0 = G'_g\Sigma\lambda/G'_{rubber}$, we obtain that K^{num} is given by

$$K^{num} = \frac{\Sigma K^{phys}}{G'_{rubber}} \tag{18}$$

If we assume $\Sigma = 0.05$, $G'_{rubber} = 5 \times 10^5$ Pa, and $K^{phys} = 10^6$ Pa K^{-1}, we obtain $K^{num} = 0.1$ K^{-1}. For these systems the Payne effect is expected for deformations ϵ_c such that $k_0\epsilon_c/K^{num} \approx 100$ K. We obtain thus $\epsilon_c \approx 10\%$. We will consider for K^{num} values varying between 0.1 and 0.3 K^{-1} in this paper.

D. Simulating Elastomers Reinforced with Filler Aggregates of More Complex Structure. The model described here is generic, in particular whatever the fillers structure. However, regarding the implementation of the model in numerical simulations, we will consider in this article that the fillers are spherical beads, which might be close to the real geometry of some systems but is a simplified one as compared to fractal aggregates. When considering real systems reinforced with such fillers, one needs thus to discuss the corresponding mapping between physical quantities and the parameters of the simulations. The mapping can be made if we assume that the simulations (performed by considering spherical beads) represent the local behavior of fractal aggregates fillers at their closest approach. In this case, the applied deformation γ has to be interpreted as the local deformation between two fillers at their closest approach. Thus, one expects the simulations to represent systems with fractal aggregates (with some limitations discussed later in the paper) also provided the corresponding deformation is rescaled according to $\gamma_{macr} = \gamma/\lambda$. If we assume for instance that $\lambda \sim 10$ (as will be the case typically for elastomers filled at high volume fraction with fillers of 100 nm diameter made by assembling beads of 10 nm diameter), it amounts to rescale the macroscopic deformation by a factor 1/10. The resulting strain softening is obtained for macroscopic deformations of order ~1% (by considering the same parameters as in section IIID), which is the case of the systems studied by Payne).[8] The modulus obtained by the simulations is then a local modulus on the scale of two closest points between fillers. To obtain the macroscopic modulus, the modulus of the simulation has to be rescaled by a factor $\lambda^{fractal}\Sigma^{fractal}/\Sigma^{beads}\lambda^{beads}$. If we assume that $\Sigma^{fractal} = 0.01$ and $\lambda^{fractal} = 10$, whereas $\Sigma^{beads} = 0.1$ and $\lambda^{beads} = 1$, the rescaling of the modulus is 1. Thus, with the parameters discussed here and which will be considered later in this paper, only the ordinate axis has to be rescaled, by a factor 0.1.

To conclude here, our simulations represent more directly, and are aimed at predicting the behavior of, elastomers filled with 10 nm spherical particles. They allow also to discuss the behavior of elastomers filled by larger fractal aggregates by an appropriate rescaling of G' and G'' (by a factor 1 with the parameters of the simulations considered in this article) and an appropriate rescaling of the deformation amplitude γ (by a factor typically 1/10 in our simulations here) to deal with 100 nm diameter fillers made by assembling spherical particles of 10 nm. Thus, we expect them also to explain the results obtained by Payne in his 1963 paper.

E. Parameters of the Simulations. The preceding discussions allow for determining how the set of parameters β, λ, Σ, K, ζ, k_0, and k_∞ used in the simulations relate to the corresponding physical quantities and for determining their values, according to the regimes of interest. The time scale is set by the WLF law of the polymer matrix. Therefore, the time unit of the simulations are expressed in seconds and represent real physical time scales. The parameters and the corresponding values used in our simulations are recorded in Table 1.

IV. Results and Discussion

A. Reinforcement. The elastic modulus G' (in units of MPa) measured at small shear amplitude ($\gamma = 5 \times 10^{-3}$) is plotted in

Table 1. Parameters of the Model[a]

parameters of the model	physical value	value in the simulation
number of particles		$N = 5000$
connectivity of springs		$n = 10$
filler volume fraction	10−40%	15−45%
fillers diameter	10 nm	$d = 1.0$
rubbery modulus	$G'_{\text{rubber}} = 5 \times 10^5$ Pa	$k_\infty = 1$
glassy modulus	10^9 Pa	$k_0 = 100$
glass transition temperature T_g of the pure rubber	213 K	$T_g = 213$ K
WLF parameters of the pure rubber	$C_1 = 12.8$; $C_2 = 34$ K	$C_1 = 12.8$; $C_2 = 34$ K
temperature of the experiment T	T	T
typical deformation rate	0.1 s^{-1}	$\dot{\gamma} = 0.1$ s^{-1}
dissipative modulus at large deformation amplitudes	10^6 Pa	$\zeta = 4$ s
coefficient β	0.2−1 nm	0.02−0.1
coefficient K	10^6 Pa K^{-1}	0.1−0.3 K^{-1}
aging coefficient	≲1	0.4

[a] In addition to the glass transition temperature of the matrix, one needs the complete WLF law of the considered polymer.

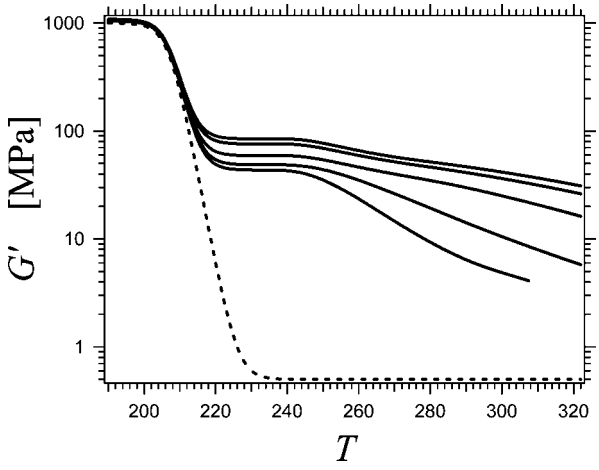

Figure 9. Elastic modulus in the linear regime (oscillatory shear of amplitude $\gamma = 0.005$ and period $T = 6.28$ s) as a function of temperature for various volume fractions Φ. Interaction parameter $\beta = 0.08$, yielding parameter $K = 0.3$, WLF parameters of polyisoprene with $T_g = 213$ K. The modulus G'_0 of the elastomer matrix (dashed curve) is modeled in such a way that $G'_0 = G'_{\text{rubber}} = 0.5$ MPa in the high temperature regime and $G'_0 = 1$ GPa on the glassy plateau below T_g. The modulus of a reinforced matrix as a function of temperature is the sum of the modulus G'_0 of the matrix plus the curve G' obtained in the simulation. The various curves from bottom to top correspond to the filler volume fractions $\Phi = 0.15$, 0.20, 0.30, 0.40, and 0.45, respectively. The discrete points, obtained at various temperatures in the simulations, have been interpolated to obtain the curves shown here. The corresponding temperatures are $T = 218$, 223, 228, 233, 238, 243, 253, 263, 283, 303, and 323 K (except in the case of the latter for the less reinforced system). Reinforcement is observed over a very wide temperature range, up to $T_g + 150$ K for $\Phi = 0.45$.

Figure 9 as a function of the temperature T, for filler volume fractions Φ varying from 0.15 to 0.45 and a value of the interaction parameter $\beta = 0.08$. The WLF parameters are those of polyisoprene, with $T_g = 213$ K.[62] The curves in Figure 9 have been obtained by adding two contributions. The contribution of the glassy bridges, which is the one obtained in the simulations and is primarily considered here, has been added to the contribution of the rubbery part of the matrix, which is shown as the dashed curve in Figure 9. The value of this latter contribution has been taken to be constant, equal to $G'_{\text{rubber}} = 5 \times 10^5$ Pa at high temperature and increases up to 10^9 Pa in a small temperature interval in the vicinity of T_g. Thus, the plateau in G' observed between about 225 and 245 K, with precise

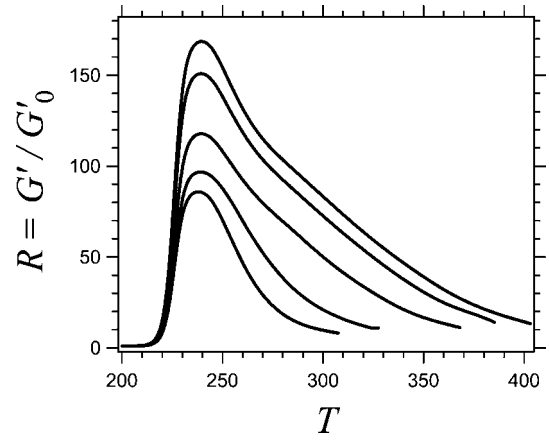

Figure 10. Reinforcement as a function of temperature. The reinforcement is defined as $R = G'/G'_0$, where G' is the modulus of the reinforced elastomer and G'_0 is that of the pure matrix. The curves from bottom to top correspond to the filler volume fractions $\Phi = 0.15$, 0.20, 0.30, 0.40, and 0.45, respectively. Interaction parameter $\beta = 0.08$. For the lower filler volume fraction $\Phi = 0.15$, no reinforcement is measured at temperatures larger than 300 K. The data are the same as in Figure 9. When relevant (depending on the filler volume fraction), they correspond to the temperatures $T = 218$, 223, 228, 233, 238, 243, 253, 263, 283, 303, 323, 343, 363, 383, and 403 K.

boundaries depending on the volume fraction Φ, is due to the contribution of glassy bridges. Real systems are not expected to exhibit this plateau, but rather a more continuous increase of the modulus as T decreases. The simulated systems show a constant modulus as soon as they enter a regime in which all filler particles are connected by glassy bridges, which are represented by springs with a constant (independent of temperature) stiffness $k_0 = 100$. This corresponds to a constant glassy fraction area Σ (see the discussion in section IIA). Real systems show a continuous increase of the glassy layer thickness, or glassy fraction, as T decreases, which corresponds to an increase of Σ as T decreases. This would correspond to an increase of the stiffness k_0 as T decreases.

The curves in Figure 9 show that a strong reinforcement, up to about 100 MPa, can be obtained over a large temperature range, which is comparable to the data obtained by Payne.[8] The main point here is that the elastic modulus is a strongly decreasing function of the temperature well above the T_g of the elastomer matrix, contrary to the case of pure elastomers. This feature has also been noticed by Payne and more recently by Berriot et al.[35−37] It is essential to note that this characteristic behavior rules out purely geometrical effects. These data may be alternatively plotted to show the reinforcement, defined as the ratio $R = G'/G'_{\text{rubber}}$ of the elastic modulus of the reinforced system to that of the pure elastomer. The reinforcement curves corresponding to the data in Figure 9 are plotted as a function of temperature in Figure 10. The reinforcement curves are plotted as a function of temperature in Figure 11 for systems with a filler volume fraction $\Phi = 0.40$ and different values of the interaction parameter $\beta = 0.02$, 0.04, and 0.08. By comparing Figure 11 to Figure 10, we see that the effect of reducing the strength of the matrix−filler interaction is qualitatively equivalent to reducing the filler volume fraction as regards the reinforcement. The reinforcement extends to a narrower temperature range for less strongly reinforced systems, which here correspond either to lower filler volume fraction Φ (Figure 10) or to lower values of the interaction parameters β (Figure 11).

The curves are strongly peaked at a temperature a few tens of kelvin above the elastomer T_g. In the series of papers by Berriot et al.,[35−38] this effect was interpreted as a consequence of the long-ranged nature of the effects of interfaces on the

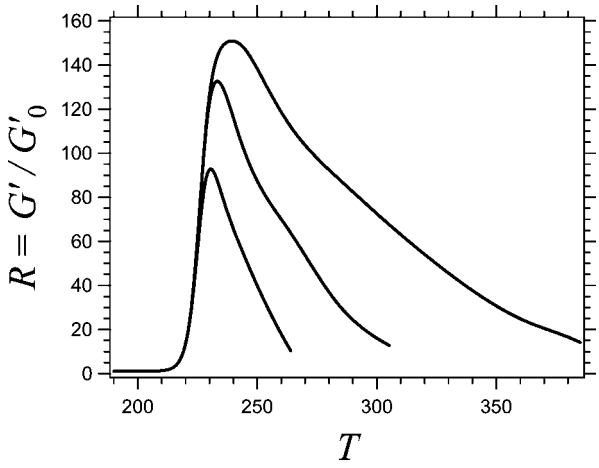

Figure 11. Reinforcement as a function of temperature for systems with filler volume fraction $\Phi = 0.4$ and different values of the interaction parameter β: from bottom to top $\beta = 0.02$, 0.04, and 0.08, respectively. When only weak filler−matrix interactions are present, no reinforcement is measured above room temperature. The discrete points, obtained at various temperatures in the simulations, have been interpolated to obtain the curves shown here. When relevant (depending on the reinforcement parameter β), the data correspond to the temperatures $T = 218$, 223, 228, 233, 238, 243, 253, 263, 283, 303, 323, 343, 363, and 383 K.

dynamics of polymer matrices. In the systems considered therein, the typical distance between particles was about 20−30 nm and the maximum of reinforcement reached a value close to 58 (with $\Phi = 19\%$) at a temperature $T \approx T_g + 7$ K. This value is more than 20 times larger than the contribution of purely geometric effects, which could be measured in the high temperature regime and were of order 3. Another effect which has been proposed for explaining reinforcement is the presence of physical interactions which link the monomers to the filler surface. It was shown that it results in an increase of the density of effective cross-links, including frozen entanglements, in the vicinity of the fillers.[65,66] However, we argue that this effect can explain neither the amplitude of reinforcement nor the long-ranged effects described in refs 35−37. Indeed, beyond a distance of the order 1 nm, the local density of effective cross-links should be at most 10^{27} m^{-3} (which is actually overestimated and in any case is much larger than the results obtained by numerical simulations in ref 66), resulting in a local elastic modulus of 4×10^6 Pa. The local elastic modulus crosses over to the bulk value G'_{rubber} of a few 10^5 Pa at a distance of 5 nm from the interface at most. This is quite smaller than the average distance between silica particles in the systems considered in refs 35−37. Silica particles would then in any case be separated by about 10 or 20 nm of elastomer with bulk property. According to the master curve for reinforcement presented in ref 37, the corresponding effective filler volume fraction would be of the order $\Phi_{eff} = 26\%$ and lead to a reinforcement of 8 at most instead of a peak at 58 for a filler volume fraction $\Phi = 19\%$ or to a reinforcement of about 3 instead of a peak at 10 for $\Phi = 10\%$. It is thus very difficult, if not impossible, to interpret the reinforcement in systems such as those studied by Berriot et al. as a consequence of an increase of the density of chain entanglements in the vicinity of fillers. Similarly, given the very high values of reinforcement observed by Payne in his 1963 study, we consider that the reinforcement that he describes is a consequence of the presence of glassy layers.

Note that we consider here systems which are more reinforced than those studied by Berriot et al. For instance, with our systems the peak in reinforcement reaches a value close to 80 (or more, depending on the systems), whereas in the systems studied by Berriot et al. the reinforcement peaks at 58. But the general feature is the same. A more precise comparison would imply to take a few of the parameters of our model (e.g., β and Φ) as fitting parameters.

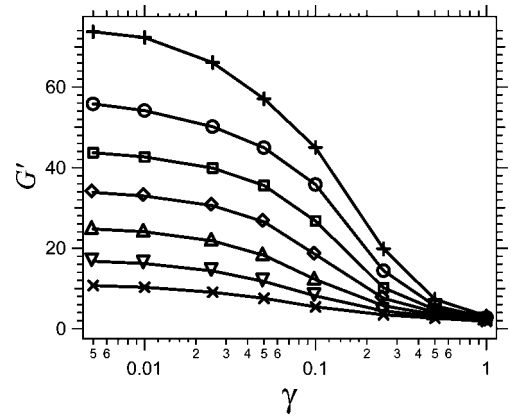

Figure 12. Elastic modulus G' (in MPa) in the simulated reinforced elastomers, measured in oscillatory shear at a pulsation $\omega = 1$ rad s^{-1}, as a function of the shear amplitude γ, at various temperatures T between 243 and 363 K: $T = 243$ K (+), 263 K (○), 283 K (□), 303 K (◇), 323 K (△), 343 K (▽), and 363 K (×). The parameters are $\Phi = 0.40$, $\beta = 0.08$, and $K = 0.3$, and WLF parameters of PI with $T_g = 213$ K.

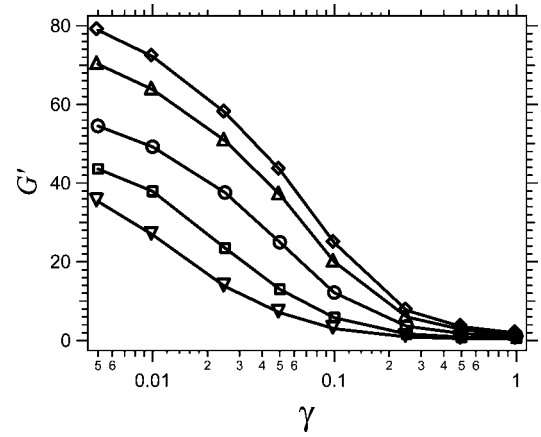

Figure 13. Elastic modulus G' (in MPa) as a function of the shear amplitude γ at $T = 243$ K for different volume fractions: $\Phi = 0.15$ (▽), 0.20 (□), 0.30 (○), 0.40 (△), and 0.45 (◇). Other parameters are $\beta = 0.08$, $K = 0.1$, pulsation $\omega = 0.2$ rad s^{-1}, and WLF parameters of PI with $T_g = 213$ K.

B. Nonlinear Behavior: Payne Effect. The elastic modulus G' obtained in the simulations is plotted in Figure 12 as a function of the oscillatory shear amplitude γ, for various temperatures between 243 and 363 K. Since the applied deformation changes the state of the system, it is important to note that G' is measured in the permanent regime after typically 10 cycles. The system is strongly reinforced, with $\Phi = 0.40$ and $\beta = 0.08$. The lower the temperature, the larger the modulus at a given deformation. One can observe a large drop of G' for deformation amplitudes of order a few percent to about 10%. We interpret the drop of elastic modulus as a progressive breaking of glassy bridges. The larger the amplitude of deformation, the larger the fraction of glassy bridges which have broken and the lower the elastic modulus. The elastic modulus G' is plotted as a function of γ in Figure 13 for various filler volume fractions Φ between 0.15 and 0.45, at a given temperature $T = 243$ K and for strong matrix−filler interactions ($\beta = 0.08$). The systems with a larger filler volume fraction Φ retain a large elastic modulus at higher strain than systems with a lower Φ. This is particularly noticeable at $\gamma \approx 10\%$, for which the system with $\Phi = 0.15$ has almost entirely lost its reinforcement

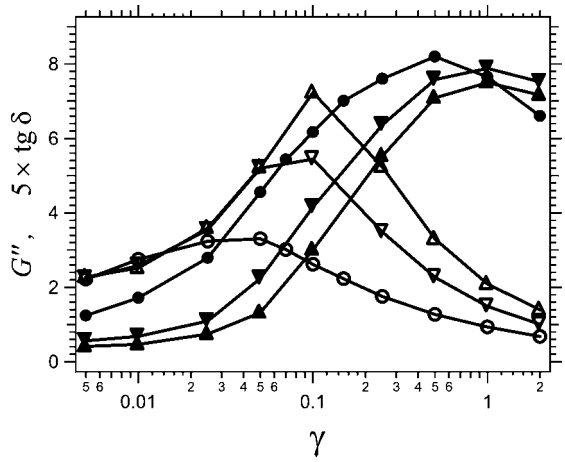

Figure 14. Loss modulus G'' (in MPa) (open symbols) and tan δ (the quantity $5 \times \tan \delta$ is plotted as filled symbols) as a function of the shear amplitude γ at $T = 283$ K for different volume fractions: $\Phi = 0.20$ (○), $\Phi = 0.30$ (▽), and $\Phi = 0.40$ (△). Other parameters are $\beta = 0.08$, $K = 0.2$, and pulsation $\omega = 0.2$ rad s^{-1}.

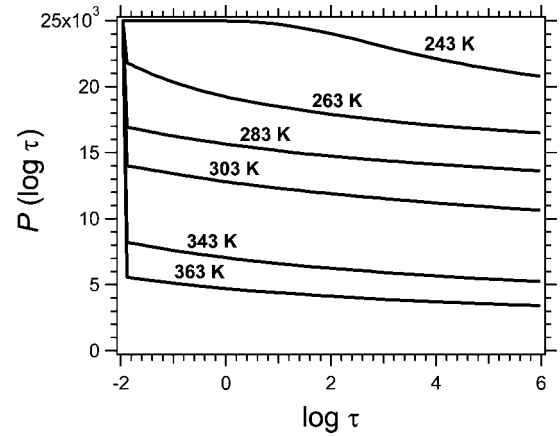

Figure 15. Distributions of relaxation times $P(\log \tau)$ at equilibrium (i.e., after infinite waiting time) at various temperatures from 243 to 363 K (top to bottom curves respectively), in the system $\Phi = 0.40$, $\beta = 0.08$, and $K = 0.3$. $P(\log \tau)$ is the number of glassy bridges with a lifetime equal to or larger than τ. τ is expressed in s. WLF parameters of PI, with $T_g = 213$ K, are used. The total number of neighboring pairs is 25 000.

whereas systems with higher filler contents still have an elastic modulus which is still much higher than that of the matrix.

The loss modulus G'', also measured in the permanent regime after about 10 cycles, and $\tan \delta(\gamma) = G''(\gamma)/G'(\gamma)$ are plotted in Figure 14 as a function of the deformation amplitude γ in systems with filler volume fractions Φ varying from 20% to 40%. G'' displays a maximum for a deformation range of the order 5−10%, which corresponds to the range in which the elastic modulus G' decreases steeply. Note that a pronounced maximum in G'' is also observed in the strongly reinforced systems which were studied by Payne.[8] We thus predict that strongly reinforced elastomers filled with 10 nm diameter fillers should exhibit a marked peak in G'' for strain amplitudes of order 10%. When considering elastomers reinforced by fillers which are fractal aggregates, a mapping can be made between our simulations and these more complex systems, if we assume that the simulations represent the local behavior of fillers at their closest approach. In this case, as discussed in section IIID, the applied deformation γ has to be interpreted as the local deformation, corresponding to a macroscopic deformation $\gamma_{macr} = \gamma/\lambda$. If we assume that $\lambda = 10$, it amounts to rescale the macroscopic deformation by a factor 1/10. The resulting strain softening and the peak of G'' are obtained for macroscopic deformations of order ∼1%, which is the case of the systems studied by Payne.[8] As discussed in section IIID, the modulus obtained in the simulation has to be rescaled by a factor 1. Our simulations allow thus to interpret semiquantitatively Payne's results[8] regarding the dependence of G' and G'' as functions of the deformation amplitude γ.

We can see in Figure 14 that $\tan \delta(\gamma) = G''(\gamma)/G'(\gamma)$ varies from a low value at small strain amplitude to a value of order 1 at large deformation amplitude when most glassy bridges break under the applied strain and goes through a maximum of order 1 for deformations of order a few 10%. The behavior at different filler volume fractions are qualitatively the same, except that the drop in elastic modulus is sharper in the $\Phi = 40\%$ reinforced system. In ref 8 Payne measured similar effects, with relatively high values for tan δ. The latter peaked at around 0.6 for strongly reinforced systems. We note that in our simulations the latter peaks at somewhat larger values, i.e., 1.3−1.4. However, the qualitative behavior and the order of magnitudes are similar. The overestimate by a factor of 2 is probably the result of both an overestimate of G'' and an underestimate of G' due to an overestimate of the rupture of glassy bridges around the inflection point of the curve $G'(\gamma)$. The latter might be due to the simplified geometry of our systems, where the fillers are represented as hard spheres, as compared to real systems where the fillers are fractal aggregates. With real systems, it is likely that more glassy bridges survive large deformation amplitudes or break over a larger deformation range γ. If more glassy bridges survive, the decrease of G' is less abrupt and the amplitude of G'' is smaller. Both trends contribute to lower tan $\delta(\gamma)$. Note however that a factor of 2 is not a large value, given the complexity of real systems and the simplified assumptions and description inherent to the modeling of filled elastomers.

C. Distribution of Breaking Times. To get more precise insight into the behavior of our systems under strain, we consider now the distribution of breaking times, both at equilibrium and under strain. $P(\tau)$ is defined as the number of bridges which have a breaking time equal to or larger than τ. The distributions of the breaking times of glassy bridges are plotted in Figure 15 at different temperatures from 243 to 363 K, in a strongly reinforced system with filler volume fraction $\Phi = 0.4$ and interaction parameter $\beta = 0.08$. The distributions at equilibrium, i.e., after an infinite waiting time, are considered here.

We see that at relatively low temperature, i.e. $T = 243$ K, more than 80% of bridges have a breaking time longer than $\tau_{max} = 10^6$ s. On increasing the temperature, the distribution of breaking times shifts toward shorter times. However, in this strongly reinforced system, even at $T = 363$ K, a fraction of order 12% of bridges still have breaking times longer than 10^6 s. The system is still strongly reinforced since this fraction is sufficient for percolating or at least gives rise to large clusters of filler particles connected by strong glassy bridges (see section IVE). The distribution of breaking times at equilibrium are plotted in Figure 16 for various filler volume fractions Φ at a temperature $T = 283$ K and for strong filler−matrix interaction ($\beta = 0.08$). One can see that the distribution of breaking times shifts toward longer times, or in other words, the fraction of bridges with a breaking time longer than $\tau_{max} = 10^6$ s increases, when increasing the filler volume fraction. This leads to larger clusters of fillers connected by strong glassy bridges and to percolation of the glassy bridges network and therefore to a stronger reinforcement. A similar behavior is observed in Figure 17 in which are plotted the distributions of breaking times for various filler−matrix interaction strength β in a system with volume fraction $\Phi = 0.40$ at $T = 263$ K. On increasing the strength β, the distribution shifts toward longer time scales, which results in an increase of the reinforcement.

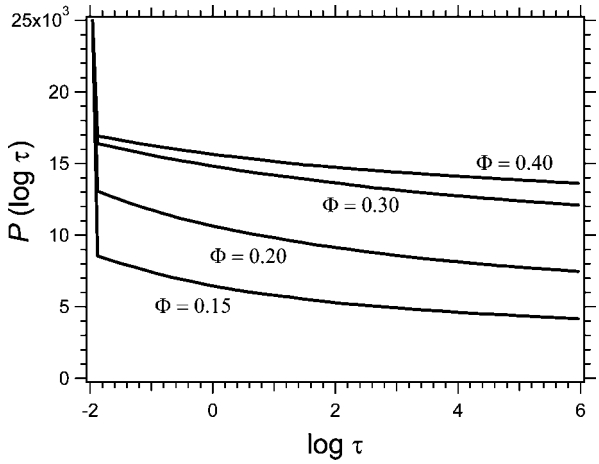

Figure 16. Distributions of relaxation times $P(\log \tau)$ at equilibrium at $T = 283$ K for various values of the volume fraction Φ from 0.15 to 0.40 (bottom to top curves, respectively) in the system $\beta = 0.08$ and $K = 0.3$. WLF parameters of PI, with $T_g = 213$ K, are used.

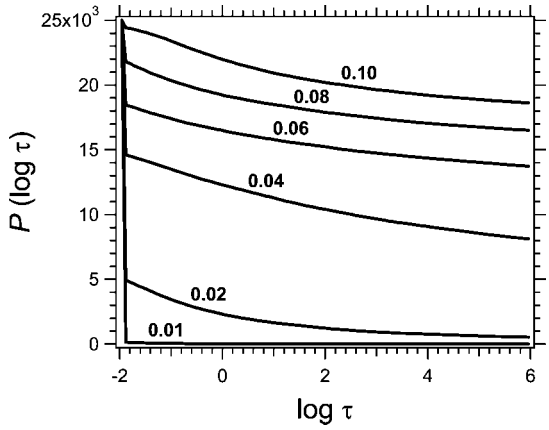

Figure 17. Distributions of relaxation times $P(\log \tau)$ at equilibrium in the system at $T = 263$ K, $\Phi = 0.40$, and $K = 0.3$ and for various values of the reinforcement parameter β from 0.01 to 0.10 (bottom to top curves, respectively; the values of β for each curve are indicated on the graph). WLF parameters of PI ($T_g = 213$ K).

When applying a deformation to a sample, local stress increases, which results in a lowering of the local T_g of glassy bridges, which means a sharp diminution of breaking times. The distribution of breaking times in a system which has been sheared at different amplitudes γ between 0.005 and 1.0 are plotted in Figure 18. One can see that for a very small deformation amplitude the distribution of breaking times is only slightly altered and remains essentially equal to the equilibrium one. At larger applied strain, the distribution shifts toward smaller time scales. It is very important to note that the distributions plotted here are the results of a birth and death process of glassy bridges, which are measured in the permanent regime of the applied oscillatory deformation, after typically 10 cycles. The shift toward shorter lifetimes results in the lowering of the elastic modulus G'. Indeed the value of G' measured for an amplitude γ is directly related to the fraction of bridges with breaking times comparable to, or larger than, the experimental time scale (here the period $2\pi/\omega$ of the oscillatory deformation). At $\gamma = 1.0$ the fraction of glassy bridges with lifetimes larger or equal to the time scale of the applied strain (of order $2\pi/\omega \sim 10$ s) has dropped to a smaller value than the equilibrium one, and as a consequence the modulus G' has dropped down to a much smaller value (not shown here for these specific systems). Considering the breaking of glassy bridges under shear helps to understand dissipative

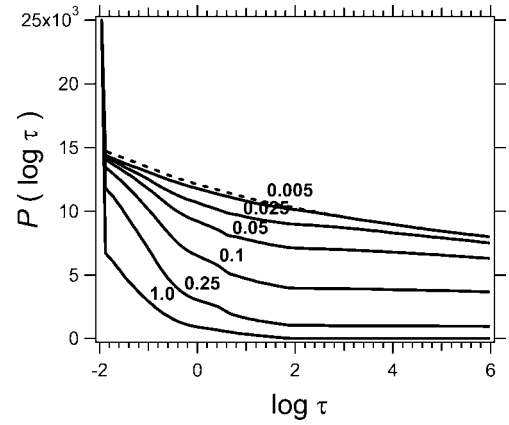

Figure 18. Distributions of relaxation times $P(\log \tau)$ after an oscillatory shear of various amplitudes γ from 0.005 to 1.0 (from top to bottom curves, respectively; the values of the shear amplitude γ for each curve are indicated on the graph), at $T = 263$ K in the system $\Phi = 0.40$, $\beta = 0.04$, and $K = 0.3$. $P(\log \tau)$ is measured after 10 cycles of pulsation $\omega = 1.0$ rad s^{-1} (period $2\pi/\omega = 6.28$ s). The upper dashed curve is the distribution at equilibrium (i.e., after infinite aging time) which is taken as the initial distribution of relaxation time in the system, prior to shearing.

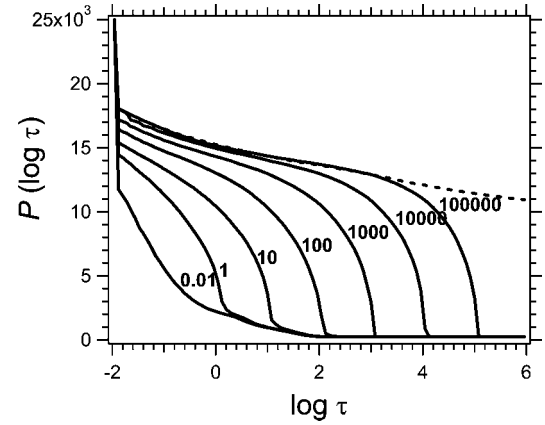

Figure 19. The system $\Phi = 0.40$, $\beta = 0.08$, and $K = 0.3$; at $T = 263$ K is sheared at large amplitude ($\gamma = 1.0$, 10 cycles, period $2\pi/\omega = 6.28$ s) and then relaxed during an aging time t_w. The distributions of relaxation times $P(\log \tau)$ (in s) at the end of the aging time are plotted for various t_w. The values of t_w (in s) for each curve are indicated on the graph. The dashed curve is the distribution at equilibrium (i.e., after infinite aging time), taken as the initial distribution.

properties of the systems as well. Consider for instance the distribution of breaking times after shearing at the amplitude $\gamma = 0.1$ (Figure 18). One can see that a significant number of bridges have a lifetime comprised between 1 and 10 s. This number corresponds to the variation of the function $P(\tau)$ between these two values. In the permanent regime, this number corresponds to bridges that build and break permanently, on the time scale of the applied oscillatory deformation. They contribute fully to the dissipation and explain the presence of the peaks in $G''(\gamma)$ observed in Figure 14 and observed as well in the experiments described by Payne.[8]

D. Modulus Recovery. Mullins Effect. Once the constraint is removed, glassy bridges start building up again. We consider here a system which has been submitted to a large amplitude ($\gamma = 1.0$) oscillatory shear and then left at zero applied stress. The distributions of breaking times, measured after waiting in the relaxed state for a varying time t_w, are plotted in Figure 19. Immediately after applying the large amplitude shear, glassy bridges are broken, as was shown already in Figure 18. As the waiting time t_w increases, long breaking times are recovered

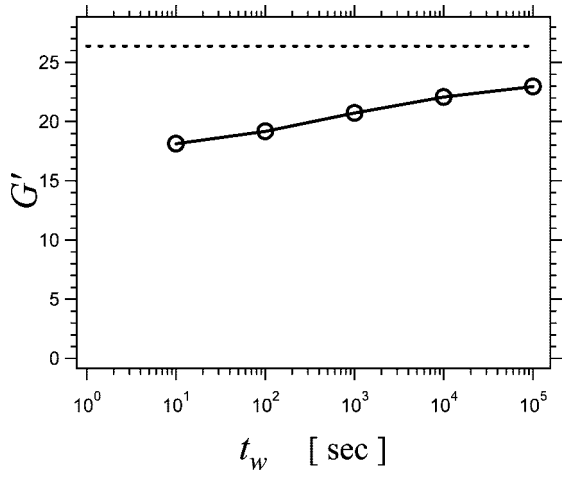

Figure 20. Partial recovery of the elastic modulus after a first large amplitude cycle. The initial system is first sheared during 10 cycles at frequency $\omega = 1\ s^{-1}$ and amplitude $\gamma = 1.0$ and then left aging at rest for 10^5 s. Then, the system is sheared again in the same way. It is then allowed to age for various times t_w, after which the elastic modulus is measured in the linear regime (at amplitude $\gamma = 0.005$). One observes a progressive recovery of the modulus for long waiting times t_w. The parameters are the following: $\Phi = 0.40$, $\beta = 0.04$, $K = 0.3$, and $T = 263$ K.

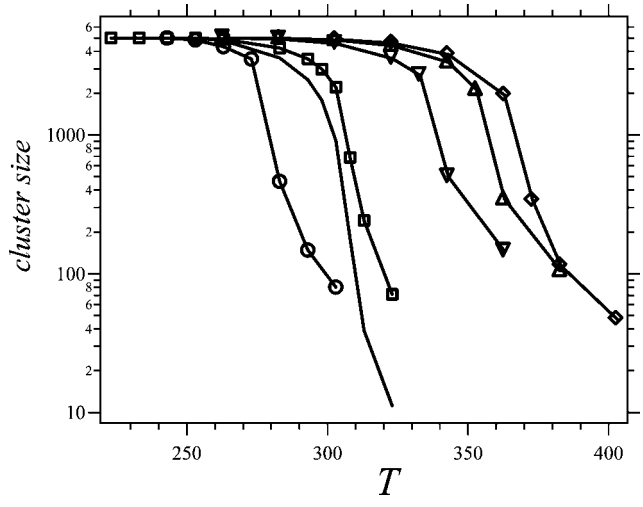

Figure 21. Mass of glassy clusters at equilibrium as a function of temperature. The mass of the largest cluster is shown for systems with various volume fractions: $\Phi = 0.45$ (◇), $\Phi = 0.40$ (△), $\Phi = 0.30$ (▽), $\Phi = 0.20$ (□), and $\Phi = 0.15$ (○). The plain curve shows the average mass $\langle m \rangle$ of glassy clusters, as defined in section IVE, as a function of temperature in the system $\Phi = 0.20$. Other parameters are $\beta = 0.08$, $K = 0.2$, and WLF parameters of polyisoprene, with $T_g = 213$ K.

progressively and the distribution evolves toward the equilibrium one, even though the latter might be impossible to reach in the experimental time scale. We interpret the experimental observation that the elastic modulus can be at least partially recovered after a first large amplitude deformation—the so-called Mullins effect—to be the result of this aging process. Note that this process also plays a key role for determining both G' and G'' in an oscillatory shear experiment, as it has been discussed above. The evolution of the elastic modulus G' after a large amplitude oscillatory shear has been applied and after the applied stress has been removed is plotted in Figure 20 as a function of the waiting time t_w. One observes indeed a slow increase of the elastic modulus as a function of the waiting time t_w. Note that Struik had also proposed that the Mullins effect was the result of the aging process of a glassy polymer layer around the fillers.[24]

E. Clusters Size. As discussed above, we argue that the elastic properties of the systems are determined by the presence of clusters of filler particles linked together by glassy bridges. Reinforcement is related to the size of these clusters. In particular, it is very strong when these clusters percolate, even though the latter condition is not imperative for obtaining a relatively strong reinforcement. The mass of a glassy cluster is defined here as the number of filler particles connected by a bridge with a relaxation time (breaking time) equal to $\tau_{max} = 10^6$ s. Note that the glass transition is a dynamical phenomenon and can be determined by an arbitrary time scale. Usually, the most relevant time scale is that of the corresponding experiment. In this article, this time scale is the period of the oscillatory deformation, typically 1 or 10 s. On the other hand, we want to consider strong glassy bridges here, i.e., bridges able to stand relatively large stress without breaking in a short time scale. These strong glassy bridges are those corresponding to the largest breaking time considered here, i.e., 10^6 s. But here also this choice is arbitrary.

The mass of the largest glassy cluster is plotted as a function of temperature in Figure 21 for various samples with different filler volume fractions Φ between 0.15 and 0.45.

An average mass of glassy clusters may be defined as

$$\langle m \rangle = \frac{\sum m^2 n(m)}{\sum m n(m)} \tag{19}$$

$n(m)$ is the number of aggregates of mass m. One has $\sum mn(m) = 5000$, which is the total number of particles in the simulations. As an example, the average mass $\langle m \rangle$ is shown in Figure 21 as a function of temperature in the system with $\Phi = 0.20$. At low temperatures, all filler particles belong to the same glassy cluster, which is of mass $m = 5000$. When temperature increases, both the average mass and mass of the largest glassy cluster decrease. For example, at $T = 320$ K, the average mass of the sample with $\Phi = 0.20$ is about 10 and the mass of the largest cluster is about 70. However, the elastic modulus at $T = 320$ K is about 10 MPa (see Figure 9), which is still a quite strong value as compared to the modulus of the matrix $G'_{rubber} = 0.5$ MPa. Even though glassy clusters no longer percolate, they are yet sufficiently large to still induce a quite strong reinforcement. Samples which remain strongly reinforced even at a relatively high temperature, e.g. 350 K, still have large glassy clusters at this temperature. Only the samples with $\Phi = 0.40$ and $\Phi = 0.45$, in which the average distance between fillers is sufficiently small, satisfy to this condition. The drop of the elastic modulus G' as the shear amplitude increases (Payne effect) may be directly related to the breaking of glassy clusters as well. The mass of the largest cluster and the average mass $\langle m \rangle$ of glassy clusters are plotted as a function of the oscillatory shear amplitude γ in Figure 22 at $T = 283$ K in a sample with $\Phi = 0.20$ and $\beta = 0.08$. One can see that both masses start decreasing for deformation larger than about 8%, which corresponds roughly to the starting point of the Payne effect. The progressive decrease of the elastic modulus of the sample is associated with a progressive decrease of the size of the glassy clusters. For a deformation of 200%, the average mass of the clusters is close to 1, which means that only small clusters of particles linked by glassy bridges survive at this high shear amplitude: in this regime, the reinforcement is essentially due to fillers steric effect and corresponds to that measured in the simulations discussed in ref 56.

Note that it would be interesting to study the spatial distribution of relaxation times, in addition to the global

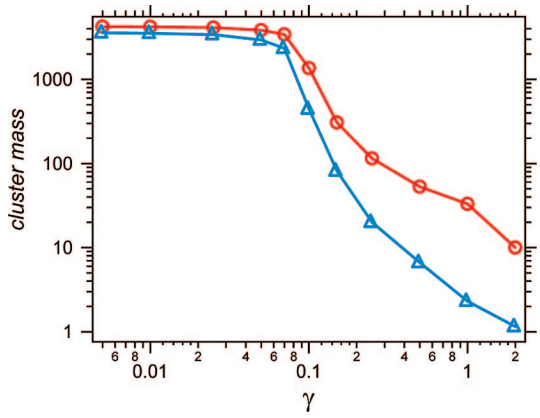

Figure 22. Mass of the largest glassy clues (○) and the average cluster mass $\langle m \rangle$ defined in section IVE (△) as a function of the oxcillatory shear amplitude γ, at $T = 283$ K in the system $\Phi = 0.20$, $\beta = 0.08$, and $K = 0.2$, at pulsation $\omega = 0.2$ rad s^{-1}. The decrease of the glassy cluster mass as γ increases is directly related to the Payne effect.

distribution that we display in Figures 15−19. In particular, the correlation function of the spatial distribution should be of interest to see whether the distribution of relaxation times is homogeneous in the material or is heterogeneously distributed, in particular under applied strain. However, the evolutions of the average mass of glassy clusters, and of the mass of the largest cluster, as a function of the deformation amplitude displayed in Figure 22 give some indication at this regard. We see that the mass of the largest cluster at 20% deformation drops to about 100, whereas the average mass is of order of a few tens. This relatively narrow difference between these two quantities indicates that the presence of large scale heterogeneities in the distribution of glassy bridges, where one would observe the presence of regions with quite large glassy clusters and other regions where all glassy bridges would have broken, are unlikely, at least for the systems considered here. More detailed and quantitative studies involving e.g. spatial correlation functions in the distribution of glassy bridges should be performed to answer precisely this question.

V. Conclusion

We have described a model for the reinforcement of filled elastomers, which should be also valid for more general nanocomposites with hard inclusions dispersed in an elastomeric matrix, such as some thermoplastic elastomers. It allows for describing the behavior of these systems both in the linear and nonlinear (nondestructive) regimes, which are the so-called Payne and Mullins effects. This model is based on the presence of glassy layers around the fillers. The presence of overlapping glassy layers results in high level of stress between fillers, with finite lifetimes. The latter depend on the history, on the temperature, on the distance between fillers, and on the local stress in the material. We have shown how the dynamics of yield and rebirth of glassy bridges account for the nonlinear behavior and dissipative properties of filled elastomers. The storage modulus is determined by the fraction of glassy bridges with lifetime comparable to or larger than the period of the oscillatory deformation, and the loss modulus is dominated by the fraction of glassy bridges with lifetimes comparable to the deformation period. These populations of glassy bridges depend on the amplitude of the deformation also. We have proposed that the Mullins effect is a consequence of an aging process of the glassy layers around the fillers.

All the parameters of the model are based on physical, measurable quantities. The model is aimed at being generic and predicts the linear and nonlinear properties of filled elastomers as a function of the polymer matrix, filler volume fraction, matrix−filler interactions, filler structure, and filler dispersion. It should apply to carbon black or silica reinforced elastomers or to thermoplastic elastomers with the relevant nanostructure corresponding to hard inclusions dispersed in an elastomeric matrix. It applies whether the fillers are beads dispersed in a matrix or fractal aggregates dispersed in the matrix, as is often the case for tires applications. Then the model was solved by numerical simulations. For these purposes, the complex structure of the filler had to be simplified, and we considered only spherical filler particles. However, we discussed how a mapping can be made between the simulations of hard beads systems and systems with more complex fractal structures. Our simulations allowed then to predict the behavior of elastomers filled with spherical beads, in the strongly reinforced regime. They allowed also for explaining semiquantitatively the results obtained by Payne in his 1963 study.[8] We could explain the amplitude of the reinforcement, the amplitude of the decrease of the elastic modulus as a function of the applied deformation and the key features of the loss modulus. We overestimated the ratio $\tan \delta(\gamma) = G''(\gamma)/G'(\gamma)$ by a factor 2, which might be a consequence of the simplified geometry (spherical beads instead of fractal aggregates) implemented in our simulations. With fractal aggregates, it is likely indeed that glassy bridges break over a larger deformation range. As a consequence the decrease of G' should be less abrupt and the amplitude of G'' smaller. Both trends contribute to lower $\tan \delta(\gamma)$. Note however that a factor of 2 is not a large value, given the complexity of these systems. In future extensions of the simulation method, one could straightforwardly deal with fractal aggregates by implementing the relevant rigid and permanent links between neighboring fillers. One could for instance simulate e.g. up to 100 aggregates of 100 beads, of diameter 10 in beads diameter unit (assuming a fractal dimension close to 2). Further extension include also representing more closely the strain rate dependence of the contribution to the dissipation of the polymer fraction which is close to the glass transition and by including explicitly a contribution of the rubbery matrix.

Note that our model relies on the validity of interfacial effects regarding the change of dynamics and in particular of the increase of glass transition temperature induced by a solid subtrate with strong interactions with the polymer as described in the literature.[25−27,33] In particular, eq 3, and the corresponding use of the WLF law, are an essential assumption of our model. The details of the T_g changes are not very important since they can be included in the adjustable parameters of the model, but the main features must be valid in order that the physics of filled elastomers can be described with values of the parameters that have a physical meaning. Conversely, our model provides a link between thin films dynamics and the behavior (linear and nonlinear) of filled elastomers. Therefore, it should help resolve the current scientific issues regarding thin films dynamics, by allowing to compare experimental results obtained regarding thin films experiments, on the one hand, to results obtained with nanofilled polymers, on the other hand. Indeed, we have shown that the strength of the interaction between the fillers and the matrix (parameter β in eq 1), which determines the T_g shift in the vicinity of the fillers, is key for controlling reinforcement properties, regarding both the elastic modulus and the dissipative modulus. Our model opens thus the way for predicting mechanical behavior of nanofilled elastomers according to the filler structures and dispersion, polymer−filler interactions, and temperature, in order to prepare systems with tailored properties.

Appendix A. Implementation of the Model

The model described above is solved numerically by overdamped dissipative particle dynamics. The implementation is performed by extending a model which we proposed re-

cently[55−57] for describing mesoscale behavior of soft thermoplastic elastomers or reinforced elastomers in the high temperature regime, when glassy layers do not overlap. The basic ingredients of the model are permanent elasticity, disorder, and excluded volume effects. The solid filler particles are represented by hard spheres randomly distributed in space. The hard sphere potential is described by

$$V_{hs}(r) = \begin{cases} F_{hs}^{max} r + H & (r < r_{min}) \\ \epsilon r^{-12} & (r_{min} < r < r_{cut}) \\ 0 & (r_{cut} < r) \end{cases} \quad (20)$$

where r is the dimensionless distance between particles. We choose $\epsilon = 1$. The force $F_{hs}(r)$ cancels beyond a cutoff distance $r_{cut} = 2$. At this distance, F_{hs} is already much smaller than ϵ. The force is bounded at short distances to prevent numerical instabilities in the initial step of the simulations, in which the centers of two particles may be very close. The constant H is chosen to ensure the continuity of the potential. $F_{hs}(r)$ rises very sharply at r of the order one. For instance, it is already of the order 20 (in units of ϵ) for $r \approx 0.96$. This means that it is quite realistic to consider $r = d = 1$ as the particle diameter. Apart from the hard sphere repulsion, two neighboring fillers interact with both elastic forces described above in section IIIA.

Periodic boundary conditions are used in order to simulate bulklike behavior. This means that a spring emanating from a particle close to a boundary and pointing out of the box is identified with a symmetrical one coming into the box and acting on another particle close to the opposite side of the box. To prepare the system, N particles are dispersed at random in a box of volume $V = L^3$ such that the volume fraction takes the chosen value Φ, that is

$$L = \left(\frac{\pi N}{6\Phi}\right)^{1/3} \quad (21)$$

The volume V of the box is kept constant throughout the simulations. The average distance between particles is then

$$a = \left(\frac{\pi}{6\Phi}\right)^{1/3} \quad (22)$$

For an average number of connections per particle n, the total number of springs in the system is $Nn/2$ (one spring contributes to two connections). Particle pairs are listed, and the $Nn/2$ closest ones are connected by springs. The equilibrium length l_0 (see section IIIA) is set equal to the average distance between neighboring sites on an ordered simple cubic lattice, that is, $l_0 = (1)/(n)(6 + (n - 6)\sqrt{2})a$ (for $6 < n < 18$), where a is the lattice parameter corresponding to the volume fraction Φ. This value for l_0 is quite arbitrary. The properties of the systems which will be investigated do not depend on this particular choice. Only the value of the pressure (the isotropic part of the stress tensor) which is applied to maintain the volume constant, depends noticeably on l_0.

The equations of the dynamics are noninertial and include a source of dissipation in the form of a hydrodynamic friction term. The equation of motion for particle i is thus

$$\vec{F}_{el}^{\,i} + \vec{F}_{hs}^{\,i} + \vec{F}_{hydro}^{\,i} = \vec{0} \quad (23)$$

To save computation time, the hydrodynamic friction $\vec{F}_{hydro}^{\,i}$ is computed in a mean field way, that is, with respect to the average affine deformation rate rather than to the actual motion relative to the surrounding of a particle. $\vec{F}_{hydro}^{\,i}$ is thus given by

$$\vec{F}_{hydro}^{\,i} = -\zeta(\vec{v}^{\,i} - \langle\vec{v}\rangle) \quad (24)$$

where $\vec{v}$ is the velocity of particle i and $\langle\vec{v}\rangle$ the average velocity of the surrounding particles. Equations 23 and 24 give the velocities at time t as a function of the positions $\vec{r}^{\,i}$:

$$\vec{v}^{\,i} = \langle\vec{v}\rangle + \frac{1}{\zeta}[\vec{F}_{el}^{\,i} + \vec{F}_{hs}^{\,i}] \quad (25)$$

The positions and velocities are computed every time interval dt. The equations of motion are solved using the modified midpoint method (MMM).[67] Quantities of interest such as the stress tensor are calculated using standard expressions,[55,68] which are summarized in the Appendix. Note that, before considering simulations per se, equilibrated samples must first be prepared as described in refs 55 and 56.

Any tensorial deformation may be applied at various strain rates in the model. In this study, we will consider oscillatory shear deformations of various amplitudes. A shear experiment is performed by imposing shear steps dγ described by the deformation tensor

$$I_d + d\Gamma_{\alpha\beta} = \begin{bmatrix} 1 & d\gamma & 0 \\ 0 & 1 & 0 \\ 0 & 0 & 1 \end{bmatrix} \quad (26)$$

followed by relaxation during Δt, such that $\dot{\gamma} = d\gamma/\Delta t$. This means that, during an elementary step, the system is first affinely deformed, and then the particle positions are allowed to relax to new positions during the time Δt. An oscillatory shear of the form $\gamma(t) = \gamma \sin \omega t$ may be applied in this way by setting $d\gamma(t) = \omega\gamma\Delta t \cos \omega t$.

The elastic modulus at pulsation ω (or frequency $f = \omega/2\pi$) is then computed as follows. When submitted to oscillatory shear, the systems stabilize in a steady state after a typical relaxation time of a few tens of seconds. However, the system may exhibit a nonlinear response, especially at high shear amplitudes. Nonlinearities of the elastic response are not discussed here. Both the strain and stress are then Fourier transformed over one period, and the complex modulus G^* is measured from the relative (amplitude and phase of the) Fourier components of stress and strain at pulsation ω.

Appendix B. Deformation of an Isotropic Solid. Virial Stress Formulation

Consider a box of volume V containing N particles. The stress tensor[69] is related to the forces exerted on the particles by the Kramers−Kirkwood formula, which provides a microscopic expression for the stress tensor:[68]

$$\sigma_{\alpha\beta} = -\frac{1}{V}\sum_i F_\alpha^i R_\beta^i \quad (27)$$

where F_α^i is the α-component of the sum of the forces exerted on particle i by other particles *of the considered sample* and R_β^i is the β-component of the position of particle i. Periodic boundary conditions in the simulation box ensure that

$$\sum_i F_\alpha^i = 0 \quad (28)$$

These boundary conditions and the fact that we consider only central forces ensure that the total torque satisfies

$$\vec{T} = \sum_i \vec{R}^i \wedge \vec{F}^i = \vec{0} \quad (29)$$

References and Notes

(1) Nielsen, L. E.; Landel, R. F. *Mechanical Properties of Polymers and Composites*; Marcel Dekker: New York, 1994.
(2) Medalia, A. I. *Rubber Chem. Technol.* **1986**, *60*, 45–61.

(3) Edwards, D. C. *J. Mater. Sci.* **1990**, *25*, 4175–4185.
(4) Harwood, J. A. C.; Mullins, L.; Payne, A. R. *J. Appl. Polym. Sci.* **1965**, *9*, 3011–3021.
(5) Kraus, G. *Rubber Chem. Technol.* **1978**, *51*, 297–321.
(6) Kraus, G. *J. Appl. Polym. Sci., Appl. Polym. Symp.* **1984**, *39*, 75–92.
(7) Medalia, A. I. *Rubber Chem. Technol.* **1978**, *51*, 437–523.
(8) Payne, A. R. *J. Appl. Polym. Sci.* **1963**, *7*, 873–885.
(9) Payne, A. R. *J. Appl. Polym. Sci.* **1965**, *9*, 1073–1082.
(10) Heinrich, G.; Kluppel, M. *Adv. Polym. Sci.* **2002**, *160*, 1–44.
(11) Kazanci, M.; Cohn, D.; Marom, G.; Migliaresi, C.; Pegoretti, A. *Composites, Part A* **2002**, *33*, 453–458.
(12) Inoue, T.; Moritani, M.; Hashimoto, T.; Kawai, H. *Macromolecules* **1971**, *4*, 500–507.
(13) Bueche, F. *J. Appl. Polym. Sci.* **1961**, *15*, 271–281.
(14) Ruzette, A.-V.; Leibler, L. *Nat. Mater.* **2005**, *4*, 19–31.
(15) Holden, G.; Kricheldorf, H. R.; Quirk, R. P. *Thermoplastic Elastomers*; Hanser Publishers: Munich, 2004.
(16) Bastide, J.; Leibler, L. *Macromolecules* **1988**, *21*, 2647–2649.
(17) Rubinstein, M.; Panyukov, S. *Macromolecules* **2002**, *35*, 6670–6686.
(18) Wang, M. J. *Rubber Chem. Technol.* **1998**, *71*, 520–589.
(19) Kaufmann, S.; Slichter, W. P.; Davis, D. D. *J. Polym. Sci., Part A2* **1971**, *9*, 829–839.
(20) Haidar, B.; Salah Deradji, H.; Vidal, A.; Papirer, E. *Macromol. Symp.* **1996**, *108*, 147–161.
(21) Tsagaropoulos, G.; Eisenberg, A. *Macromolecules* **1995**, *28*, 6067–6077.
(22) Tsagaropoulos, G.; Eisenberg, A. *Macromolecules* **1995**, *28*, 396–398.
(23) Tsagaropoulos, G.; Kim, J.-S.; Eisenberg, A. *Macromolecules* **1996**, *29*, 2222–2228.
(24) Struik, L. C. E. *Polymer* **1987**, *28*, 1521–1533.
(25) Wallace, W. E.; van Zanten, J. H.; Wu, W. L. *Phys. Rev. E* **1995**, *52*, R3329.
(26) van Zanten, J. H.; Wallace, W. E.; Wu, W. L. *Phys. Rev. E* **1996**, *53*, R2053.
(27) Grohens, Y.; Brogly, M.; Labbe, C.; David, M.-O.; Schultz, J. *Langmuir* **1998**, *14*, 2929–2932.
(28) Keddie, J. L.; Jones, R. A. L.; Cory, R. A. *Europhys. Lett.* **1994**, *27*, 59–64.
(29) Mattsson, J.; Forrest, J. A.; Borjesson, J. *Phys. Rev. E* **2000**, *62*, 5187–5200.
(30) Hall, D. B.; Dhinojwala, A.; Torkelson, J. M. *Phys. Rev. Lett.* **1997**, *79*, 103–106.
(31) Long, D.; Lequeux, F. *Eur. Phys. J. E* **2001**, *4*, 371–387.
(32) Merabia, S.; Long, D. *Eur. Phys. J. E* **2002**, *9*, 195–207.
(33) Merabia, S.; Sotta, P.; Long, D. *Eur. Phys. J. E* **2004**, *15*, 189–210.
(34) Sotta, P.; Long, D. *Eur. Phys. J. E* **2003**, *11*, 375–388.
(35) Berriot, J.; Lequeux, F.; Montes, H.; Monnerie, L.; Long, D.; Sotta, P. *J. Non-Cryst. Solids* **2002**, *307*, 719–724.
(36) Berriot, J.; Montes, H.; Lequeux, F.; Long, D.; Sotta, P. *Macromolecules* **2002**, *35*, 9756–9762.
(37) Berriot, J.; Montes, H.; Lequeux, F.; Long, D.; Sotta, P. *Europhys. Lett.* **2003**, *64*, 50–56.
(38) Montes, H.; Lequeux, F.; Berriot, J. *Macromolecules* **2003**, *36*, 8107–8118.
(39) Ellison, C. J.; Torkelson, J. M. *Nat. Mater.* **2003**, *2*, 695–700.
(40) Ciprari, D.; Jacob, K.; Tannenbaum, R. *Macromolecules* **2006**, *39*, 6565–6573.
(41) Bodiguel, H.; Fretigny, C. *Macromolecules* **2007**, *40*, 7291–7298.
(42) Putz, K.; Krishnamoorti, R.; Green, P. F. *Polymer* **2007**, *48*, 3540–3545.
(43) Kropka, J. M.; Putz, K. W.; Pryamitsyn, V.; Ganesan, V.; Green, P. F. *Macromolecules* **2007**, *40*, 5424–5432.
(44) Lee, J.-Y.; Su, K. E.; Chan, E. P.; Zhang, Q.; Emrick, T.; Crosby, A. J. *Macromolecules* **2007**, *40*, 7755–7757.
(45) Bansal, A.; Yang, H.; Li, C.; Cho, K.; Benicewicz, B. C.; Kumar, S. K.; Schadler, L. S. *Nat. Mater.* **2005**, *4*, 693–698.
(46) Rao, Y.-Q.; Pochan, J. M. *Macromolecules* **2007**, *40*, 290–296.
(47) Rittigstein, P.; Priestley, R. D.; Broadbelt, L. J.; Torkelson, J. M. *Nat. Mater.* **2007**, *6*, 278–282.
(48) Schadler, L. S. *Nat. Mater.* **2007**, *6*, 257–258.
(49) Gusev, A. A. *Macromolecules* **2006**, *39*, 5960–5962.
(50) Kalfus, J.; Jancar, J. *Polymer* **2007**, *48*, 3935–3937.
(51) Starr, F. W.; Schroder, B. T.; Glotzer, S. C. *Macromolecules* **2002**, *35*, 4481–4492.
(52) Gusev, A. A. *Phys. Rev. Lett.* **2004**, *93*−4.
(53) Baeurle, S. A.; Usami, T.; Gusev, A. A. *Polymer* **2006**, *47*, 8604–8617.
(54) Baeurle, S. A.; Hotta, A.; Gusev, A. A. *Polymer* **2005**, *46*, 4344–4354.
(55) Long, D.; Sotta, P. In *IMA Volume in Mathematics and Its Applications: Modeling of Soft Matter*; Calderer, M.-C. T., Terentjev, E. M., Eds.; Springer: New York, **2005**; Vol. 141, pp 205−234.
(56) Long, D.; Sotta, P. *Macromolecules* **2006**, *39*, 6282–6297.
(57) Long, D.; Sotta, P. *Rheol. Acta* **2007**, *44*, 1029–1044.
(58) Bogoslovov, R. B.; Roland, C. M.; Ellis, A. R.; Randall, A. M.; Robertson, C. G. *Macromolecules* **2008**, *41*, 1289–1296.
(59) Robertson, C. G.; Lin, C. J.; Rackaitis, M.; Roland, C. M. *Macromolecules* **2008**, *41*, 2727–2731.
(60) Wu, S. *Polym. Int.* **1992**, *29*, 229–247.
(61) Ferry, J. D. *Viscoelastic Properties of Polymers*; Wiley: New York, 1980.
(62) Mark, J. E. In *Physical Properties of Polymers Handbook*; American Institute of Physics: New York, 1996.
(63) Merabia, S.; Long, D. *J. Chem. Phys.* **2006**, *125*, 234901.
(64) Ward, I. M. *J. Mater. Sci.* **1971**, *6*, 1397–1417.
(65) Sternstein, S. S.; Zhu, A.-J. *Macromolecules* **2002**, *35*, 7262–7273.
(66) Vladkov, M.; Barrat, J.-L. *Macromolecules* **2006**, *40*, 3797–3804.
(67) *Numerical Recipes in C, The Art of Scientific Computing*; Cambridge University Press: Cambridge, 1992.
(68) Doi, M.; Edwards, S. F. *The Theory of Polymers Dynamics*; Clarendon Press: Oxford, 1986.
(69) Landau, L. D.; Lifshitz, E. M. *Elasticity*; Pergamon Press: New York, 1993.

MA8014728